Graduate Theses and Dissertations

Graduate School

3-31-2017

Plasmonic Stimulation of Electrically Excitable Cells

Fnu Parveen
University of South Florida, parveen1@mail.usf.edu

Follow this and additional works at: http://scholarcommons.usf.edu/etd

Part of the Biomedical Engineering and Bioengineering Commons

Plasmonic Stimulation of Electrically Excitable Cells

by

Parveen

A dissertation submitted in partial fulfillment
of the requirements for the degree of
Doctor of Philosophy in Chemical Engineering
Department of Chemical and Biomedical Engineering
College of Engineering
University of South Florida

Co-Major Professor: Robert D. Frisina, Ph.D.
Co-Major Professor: Venkat R. Bhethanabotla, Ph.D.
Joseph P. Walton, Ph.D.
Nathan D. Gallant, Ph.D.
John Kuhn, Ph.D.

Date of Approval:
March 7, 2017

Keywords: Gold Nanoparticles, Nanoelectrodes, Neural Modulation, Visible Light, Prosthetics

ACKNOWLEDGMENTS

I would like to express my deepest appreciation to Profs. Robert Frisina, Venkat Bhethanabotla and Joseph Walton for their valuable guidance and persistent help during the project. I would like to thank Drs. Bo Ding and Xiaoxia Zhu for teaching me various experimental procedures for working with tissue culture and biological cells, and for their technical help in setting up my experimental equipment.

Also, I would like to thank my lab mates; Dr. Xiaolan Tang, Elliott Brecht, Andrea Lowe, Tanika Williamson and Nicole Febles for their help in experiments and having a pleasant environment in the lab.

Many thanks to Prof. Eric Bennett from the USF Medical School for giving me hands-on experience for the patch clamp technique in his lab, and Dr. Zhanna Vysotskaya, a Postdoc from Prof. Bennett's lab for providing critical ideas to get going in my initial patch clamp experiments. I am grateful to Prof. Wei Chen and his PhD student, Clausell Mathis for giving me initial patch clamp training in their lab. I am very thankful to Adriana (PhD Scholar, Cognitive and Neuroscience Department) for providing the cardiomyocyte tissue.

My sincere thanks to Robert Buzzeo, Scientific Researcher, Biosciences for letting me borrow his pipette puller, to Prof. Chris Passaglia for letting me borrow a micromanipulator from his lab, and to Dr. Tim Fawcett, Sr. Research Engineer, College of Engineering for helping me in designing the laser controller system with its LabView controlling software. Last but not least, I would like to all my friends at USF who helped me during the project. I am very grateful to my family who encouraged me to pursue higher studies at the University of South Florida - Tampa.

TABLE OF CONTENTS

LIST OF FIGURES

iv

ABSTRACT

There is a compelling need for the development of new sensory and neural prosthetic devices which are capable of more precise point stimulation. Current prosthetic devices suffer from the limitation of low spatial resolution due to the non-specific stimulation characteristics of electrical stimulation, i.e., the spread of electric fields generated. We present a visible light stimulation method for modulating the firing patterns of electrically-excitable cells using surface plasmon resonance phenomena. In in-vitro studies using gold (Au) nanoparticle-coated nanoelectrodes, we show that this method (substrate coated with nanoparticles) has potential for incorporating the technology into neural stimulation prosthetics, such as cochlear implants, with arbitrarily high spatial resolution. Au nanoparticles (NPs) were coated on micropipettes using aminosilane linkers; and these micropipettes were used for stimulating and inhibiting the action potential firing patterns of SH-SY5Y human neuroblastoma cells and neonatal cardiomyocytes. Our findings pave the way for development of biomedical implants and neural testing devices using nanoelectrodes capable of temporally and spatially precise excitation and inhibition of electrically-excitable cellular activity.

1 INTRODUCTION

The increase in average life expectancy is considered a remarkable achievement of biomedical research during the 20th century. There is a growing demand for neural and sensory prosthetic devices, for both diagnostics and treatments among our growing, aging population. The neural prosthetic devices used to measure, diagnose or restore normal function of partial or completely lost neural activity operate on the principle of electrical stimulation, e.g., cochlear implants (Wilson et al., 1991), retinal implants (Hornig et al., 2005), cardiac pacemakers (Epstein et al., 2008), etc. As per FDA analysis (December 2012), there have been over 96,000 cochlear implants in the US alone and nearly 400,000 cochlear implants worldwide since first approved for general use in 1985. Among implant patients in US, 60 % are adults and 40 % are children (17 years or younger; where 66 % of these children are 5 years or younger). There are over 3 million people worldwide with cardiac pacemakers and each year 600,00 are added, with most patients aged over 60 years (Wood and Ellenbogen, 2002). The electric fields produced by applied electric currents spread significantly in the space, resulting in low spatial resolution. There is an urgent need to look for alternative methods for neural stimulation which could address the critical issue of improved spatial resolution.

The aim of this project is to develop an alternative technology to electrical stimulation with a special focus on stimulation of neurons and cardiomyocytes, with initial emphasis on novel cochlear implant designs for deaf persons. For example, cochlear implants have an array of electrodes that are placed into the cochlea. Different electrodes stimulate different auditory nerve fibers (ANFs) via current pulses based on the sound frequencies present in the acoustic stimulus; high frequencies towards the base of the cochlea and low frequencies towards the apex of the cochlea, thus, mimicking the tonotopic (or cochleotopic) organization of the cochlea. Because of current

1

spread, despite recent technological advancements, it is difficult to stimulate discrete ANFs according to their sensitivity to different sound frequencies. Specifically, the processing of speech in background noise and musical sounds to the desired perception levels of cochlear implant users still remains a significant problem to be addressed because, normally, speech and music sounds have a wide frequency range with important temporal features, at various sound volume/intensity levels. (Firszt et al., 2007; Frisina and Frisina, 1997; Limb and Roy, 2014; O'Leary et al., 2009).

The present project also aims at developing novel stimulation/measurement systems for peripheral neuropathy; i.e., the conditions related to damage and/or malfunctioning of a nerve or a group of nerves of the peripheral nervous system. Specifically, electromyography is one of the most common techniques used to detect or diagnose peripheral neuropathy. Like cochlear implants, electromyography also works on the principle of electrical stimulation of muscles/nerves. In this method, an electrical signal through an electrode stimulates the muscles/nerves, then, electrical activity is recorded from the muscles/nerves. As electrical stimulation is not specific, it will not stimulate a single nerve but large groups of peripheral nerve bundles, and often evoke painful sensations. The annual cost of electromyography is approximately 2.8 billion dollars in US alone.

Along with sensory implants and testing devices, electrical stimulation is bench mark method to treat some neurological disorders where inhibition is needed like brain trauma or epilepsy, and for some studies of brain function. Because of such wide spread use of artificial neural stimulation, there is crucial need to look for alternative stimulation methods that would address the issue of specific point stimulation, and be utilized for the development of second generation sensorineural prosthetic devices. Interestingly, there are recent reports that infrared lasers can invoke *in-vivo* responses in peripheral nerves. For instance, Wells et al. (2005) reported 2 to 10 μm wavelength infrared lasers invoked responses from rat sciatic nerve. The likely mechanism of infrared stimulation is a temperature rise due to photothermal interactions and membrane capacitance changes (Shapiro et al., 2012; Wells et al., 2007a). Infrared lasers can also be used to stimulate ANFs of deaf animals, potentially giving better spatial resolution as compared to electric stimulation (Izzo

2

et al., 2006, 2007a,b; Littlefield et al., 2010; Rajguru et al., 2010). Shapiro et al. (2012) showed that the absorption of infrared laser energy cause a local temperature rise which does not effect a particular membrane channel directly, but changes the cell membrane capacitance. However, a major limitation of infrared lasers is that, along with the neurons, the infrared laser heats up the surrounding tissue as well, which can cause thermal damage or unwanted stimulation.

Nanoparticles are a fundamental building block of nanotechnology systems and find applications in various fields like electronics (Shipway et al., 2000), chemical (Daniel and Astruc, 2004), catalysis (Crooks et al., 2001), pharmaceuticals (Otsuka et al., 2003), biology (Salata, 2004), etc. Nanoparticles are defined as particles having a diameter less than 100 nm (Kruis et al., 1998). Their physical and chemical properties change dramatically with particle size and shape. Metal nanoparticles like gold (Au) have strong surface interactions with electromagnetic fields because of the relative availability of free electrons in conduction bands. Light, an electromagnetic wave, interacts with metal nanoparticles, conduction band electrons then oscillate, and the oscillation becomes maximum at a particular wavelength of light. This phenomenon is called surface plasmon resonance (SPR). The SPR peak can be tuned with particle size and shape. For gold nanoparticles, an SPR peak occurs around 520 nm; and Au nanoparticles absorb and scatter very efficiently. For small size particles ($<$ -20 nm in diameter), most of the light energy is absorbed by nanoparticles. As size increases, scattering efficiency increases because higher order electron oscillations start to play a significant role. As Au nanoparticles are not good emitters of light, absorbed light generates heat (Coronado et al., 2011; Huang and El-Sayed, 2010). This localized generation of a temperature gradient due to SPR is also known as plasmonic heating. Thus, for local heating applications small size Au particles (20 nm and smaller) are used, while for scattering applications like imaging, larger particles are utilized (30 nm and larger).

3

1.1 Nanomaterial-Assisted Neural Stimulation

Recently, nanomaterials have gained attention in addressing the issue of specific focal neural stimulation (Colombo et al., 2016; Deisseroth, 2015; Wang and Guo, 2016) . Recent reports have demonstrated that nanomaterials can be used for modulation of neural activity, with some reporting neural activation (Carvalho-de Souza et al., 2015; Eom et al., 2014; Zhao et al., 2009) and some reporting neural inhibition (Li et al., 2015; Yoo et al., 2014). In the studies of nanomaterial-enabled neural stimulation, different power sources have been employed to activate nanomaterials, e.g., magnetic fields (Chen et al., 2015; Huang et al., 2010), ultrasound (Marino et al., 2015), and laser light - infrared or less commonly, visible (Carvalho-de Souza et al., 2015; Farah et al., 2013; Lugo et al., 2012; Pappas et al., 2007), or near infrared (Eom et al., 2014; Li et al., 2015; Yong et al., 2014; Yoo et al., 2014). Based on initial investigation, light activation looks to be the most promising among all.

1.1.1 Nanoparticle-Enabled Neural Activation

Carvalho-de Souza et al. (2015) stimulated dorsal root ganglion (DRG) neurons from neonatal rats using ligand-conjugated Au nanoparticles with a 532 green laser light stimulation. Au nanoparticles have conjugated with three different ligands - a synthetic molecule based on the Ts1 neurotoxin (binds with voltage-gated sodium channels), antibodies targeting the TRPV1 channel-rhodopsin channels, and antibodies targeting $P2X_3$ receptor ion channels. These ligands bind to DRG neurons, and action potentials were recorded in response to 532 nm green laser stimulation. The authors attributed initiation of action potentials to membrane capacitance changes due to plasmonic heating, similar to what was shown by Shapiro et al. (2012) for infrared stimulation. In a similar vein, Yong et al. (2014) demonstrated activation of rat primary auditory neurons *in-vitro* with the help of silica-coated Au nanorods and 780 nm near-IR laser stimulation. The primary neurons were cultured from neonatal rats and incubated with nanoparticles - silica coated Au

4

nanorods and silica-coated Au nanoparticles, overnight. Au nanorods shows much higher current responses as compared to neurons incubated with Au nanoparticles. The authors attributed the responses to heat generation due to interactions of the Au nanorods and near-infrared laser. This heats leads to cell membrane capacitance changes and mechanisms similar to those proposed by Shapiro et al. (2012). Additionally, Eom et al. (2014) recorded compound nerve action potentials from rat sciatic nerve to which Au nanorods were attached, in response to 980 nm IR laser light. Nanorods were injected into the sciatic nerve using a glass capillary and subsequently, the nerve bundle was excised. The magnitudes of recorded compound action potentials were more than 6 times higher in the presence of Au nanorods compared to the control situation - no Au nanorods, IR stimulation alone. The magnitude of the compound nerve action potentials also increased with increases in laser power. The mechanism responsible was again attributed to the heat generated due to interactions of Au nanorods and 980 nm IR laser light.

1.1.2 Nanomaterials-Assisted Neural Inhibition

Yoo et al. (2014) used Au nanorods to record inhibitory response from rat hippocampal tissues. The Au nanorod surfaces were coated with polyethylene glycol (PEG) molecules by reacting the Au nanorods solution with biterminal PEG (NH_2-PEG(5K)-SH). PEG coating facilitates the binding of Au nanorods with the cell membrane, when neurons were treated with PEG-coated Au nanorods. Neural networks were cultured on a multi-channel multielectrode array chip and incubated with PEG-coated Au nanorods. A fiber-coupled 785 nm near infrared laser was used to stimulate the hippocampal neurons. There was a significant decrease in spontaneous activity when Au nanorod treated neurons were irradiated with the near infrared laser. There was a minimal change in spike activity for infrared stimulation alone, or Au nanorod treatment alone. The authors' hypothesize that heat sensitive potassium channels, such as TREK-1 were responsible for the suppression of neural activity. The heat was delivered at the nanoscale level, generated during interaction of the near infrared laser and Au nanorods. Similarly, Li et al. (2015) utilized

5

photosensitive poly(N-isopropylacrylamide) hydrogels embedded with polypyrole nanoparticles to release biomolecules (glutamate & DNQX), and neural activity was recorded in response to 980 nm infrared (IR) laser light stimulation. The hydrogel was used to release neurotransmitter - glutamate, locally near the hippocampal neurons and increases in spike activity were observed for the hydrogel, as compared to the control condition - no glutamate. Equivalent *in-vivo* studies were performed in rat visual cortex; there was a significant decrease in spikes rates when microgel loaded with an inhibitory biomolecule 6,7-dinitroquinoxaline-2,3-dione (DNQX), was applied.

1.2 Current Project

For the current project, a primary question to be investigated was: can localized plasmonic heating be used to stimulate electrically excitable biological cells such as neurons or cardiomy-ocytes? Specifically, in the present work, we investigate the stimulation of cardiomyocytes from neonatal rats, and SH-SY5Y neurons, using Au nanoparticle coated glass micropipettes and 532 nm green visible light. Because plasmonic heating is a localized phenomenon, it does not spread like electrical stimulation. So, it can potentially give higher spatial resolution than electrical stimu-lation and prosthetic devices based upon plasmonic phenomena can potentially perform better than current devices. Another advantage is that unlike electrical stimulation, plasmonic heating does not require any wire connections between the Au nanoparticles and energy source, i.e., the laser. Also, the laser does not heat up surrounding tissue like infrared stimulation. Given these potential advan-tages, plasmonic stimulation can revolutionize the existing field of biomedical stimulation implants and other therapeutic or testing systems.

In the next part of the report, experimental methods are present, followed by a discussion of experimental results. In the final part of the report, future work clinical translational pathways are presented.

2 EXPERIMENTAL METHODS

2.1 Synthesis of Gold Nanoparticles

Au nanoparticles were synthesized by bottom up approach; particles are synthesized from atoms. In a standard citrate method, a gold salt solution (Chloroauric acid) was reduced using a trisodium citrate solution (Nath and Chilkoti, 2002). Specifically, the glass beakers were washed thoroughly first with distilled water, then, with ethanol. 20 ml of 1 mM gold (III) chloride trihydrate ($HAuCl_4.3H_2O$) was boiled on a heating plate with continuous stirring, using a magnetic stirrer. Next, 2-3 ml of 1% trisodium citrate solution was added to the boiling solution of chloroauric acid. After 10 min, the solution became a deep red in color as shown in figure 2.1, which indicates the presence of Au nanoparticles.

2.2 Fabrication of Nanoelectrodes for Stimulation

Nanoelectrodes were fabricated by coating Au nanoparticles onto glass micropipettes. Nath and Chilkoti (2002) studied the interaction of a biomolecule with a monolayer of Au nanoparticles coated onto glass coverslips. This coating involved three steps: cleaning the glass coverslip surface, functionalization of the glass surface with γ-(aminopropyl) triethoxysilane, and finally, coating of the functionalized glass surface with gold nanoparticles. We used the same three steps to coat gold nanoparticles onto glass micropipettes, as explained next.

7
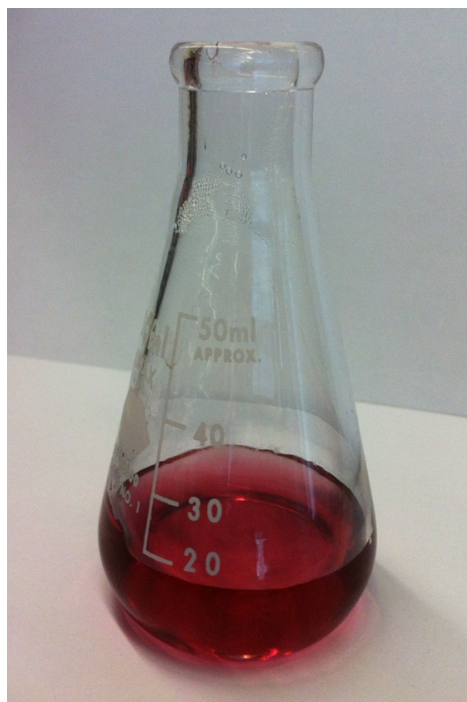
Figure 2.1: The gold nanoparticle solution that was synthesized by reduction of 1 mM gold salt solution (chloroauric acid) with a 1% sodium citrate solution. The deep red color indicates the presence of gold nanoparticles.

2.2.1 Cleaning of Micropipettes

The glass micropipettes were put inside a petri-dish and washed using liquid detergent with continuous heating at $55 - 60\,^\circ$C for 10-15 min. The micropipettes were thoroughly washed with distilled (DI) water to remove detergent. The micropipette was cleaned with 1:1 v/v (volume/volume) solution of HCl and methanol for 30 min, and subsequently, washed with DI water thoroughly. Micropipettes were dried overnight at $60\,^\circ$C in an oven.

2.2.2 Functionalization of the Micropipettes with γ-(Aminopropyl) Triethoxysilane

The tip of the micropipette was immersed in 10% v/v solution of γ-(aminopropyl) triethoxysilane in anhydrous ethanol for 15 min. Subsequently, the micropipette was washed 5 five times with ethanol and dried at $120\,^\circ$C for 3 h.

8

2.2.3 Coating of Gold Nanoparticles

The functionalized micropipette tip was immersed in the gold nanoparticles solution for 24 h. The gold nanoparticle coated micropipette was characterized using scanning electron microscopy.

2.3 Testing of Nanoelectrode

Prior to cellular physiology experiments, nanoelectrode responses to 532 nm green lasers were tested in electrochemical cells. Lowe et al. (2003) demonstrated that a laser-induced temperature jump occurs when a gold nanoparticles-coated indium tin oxide electrode was illuminated with a 532 nm green laser in a electrochemical cell, where, 0.1 M phosphate buffer containing 0.05 M EDTA was used as the electrolyte solution. The maximum photocurrent was reported near the oxidation peak potential of EDTA on gold nanoparticles, 0.9 V vs $Ag_{(s)}$/AgCl. The nanoeletrode, i.e., the microelectrode coated with the gold nanoparticles, and a Pt electrode, were used as the two electrodes of the electrochemical cell whereas a saturated calomel electrode served as the reference electrode. Figure 2.2 shows the schematic diagram of the testing set-up and the inset shows the digital micrograph the same - electrochemical cell with two electrodes, along with the reference electrode. The control experiment was done with the microelectrode not coated with the gold nanoparticles. The same experiment was done again with extracellular solution as the electrolyte instead of phosphate buffer.

Due to SPR, gold nanoparticles are known to affect the emission spectra of fluorophores in its vicinity via energy transfer between the two and are utilized in many fluorescence-based applications like molecular imaging, and sensing (Aslan et al., 2007; Aslan and Pérez-Luna, 2004; Dulkeith et al., 2002, 2005; Lee et al., 2008; Schneider et al., 2006). Aslan et al. (2007)studied the effect of Au NP size on emission spectra of FITC-labeled human serum albumin. We adapted the same methods for testing the nanoelectrodes for fluorescence quenching by the Au NPs (Aslan et al., 2007; Aslan and Pérez-Luna, 2004). FITC-labeled human serum albumin (HSA) was at-

tached to the Au NP-coated micropipette by incubating the nanoelectrode with a 10 M solution of

the fluorophore. A 488 nm laser source was used to excite FITC-HSA and the emission spectrum

the wavelength of around 520 nm was observed under an Olympus BX61W1 upright microscope.
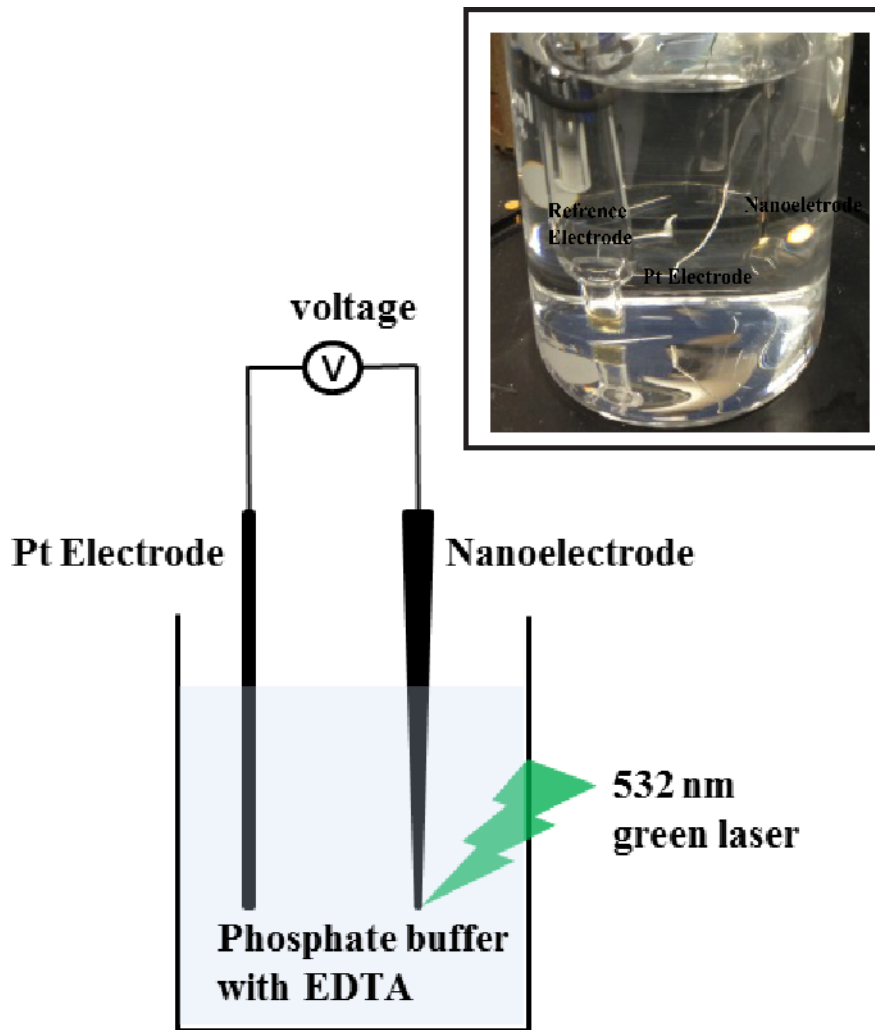
Figure 2.2: Schematic shows an electrochemical cell to record the photocurrent: A beaker filled with 0.1 M phosphate buffer/0.05 M EDTA electrolyte solution; containing both electrodes, nano-electrode and Pt electrode. The inset shows the digital micrograph of the same - two electrodes of the electrochemical cell along with reference electrode: saturated calomel electrode (SCE).

2.4 Plasmonic Temperature Measurement

Yao et al. (2009) reported a pipette resistance method, an indirect method to measure the local rapid temperature jumps occurring during the infrared stimulation of biological cells. In this method, a patch pipette filled with extracellular solution was placed in a petri dish containing the same extracellular solution and an infrared laser was focused on the tip of the pipette with the help of an optical fiber. The pipette tip was placed near the fiber, approximately at a distance equal to the distance between the fiber and cell for stimulation experiments. The resistance of the pipette was measured in response to a current pulse. A sudden change in resistance was obtained when the infrared laser pulse was applied on to the tip of the pipette. A pipette resistance vs. temperature calibration curve was obtained by putting the pipette filled with extracellular solution into a petri dish containing hot extracellular solution and allowing it to cool down. The resistances measured during infrared laser experiment were converted into temperature changes using the calibration curve (Shapiro et al., 2012).

In the present investigation, the same method was used to measure the plasmonic temperature change on the surface of nanoelectrode when a 532 nm green laser was focused on the tip of the nanoelectrode using an optical fiber having a 50 μm inside diameter. The experiment was done using our patch clamp system as shown in figure 2.3 (Multiclamp 700B amplifier and Digidata 1440A data acquisition system from Molecular Devices). The resistance vs. temperature calibration curve was obtained by allowing the extracellular solution to cool down from approximately 55 °C to room temperature. As the extracellular solution cooled down, corresponding patch pipette resistances were measured in response to a 20 mV voltage pulse. Then, a patch pipette having 5-8 MΩ resistance, filled with extracellular solution was placed very near to the surface of the nanoelectrode, and changes in resistance were measured when a 532 nm green laser was focused on the tip of the nanoelectrode. The control experiment was done without the nanoelectrode, and no resistance change was observed in response to a 20 mV pulse. Figure 2.4 shows the experiments schematic for plasmonic temperature measurements. Figure 2.5 shows the digital micrographs for

11

plasmonic temperature measurements: a) plasmonic temperature measurement and b) the control experiment. Plasmonic temperature rises were also confirmed using an infrared thermal camera (FLIR T420 thermal camera with detector spectral range 7.5 to 13.0 μm).
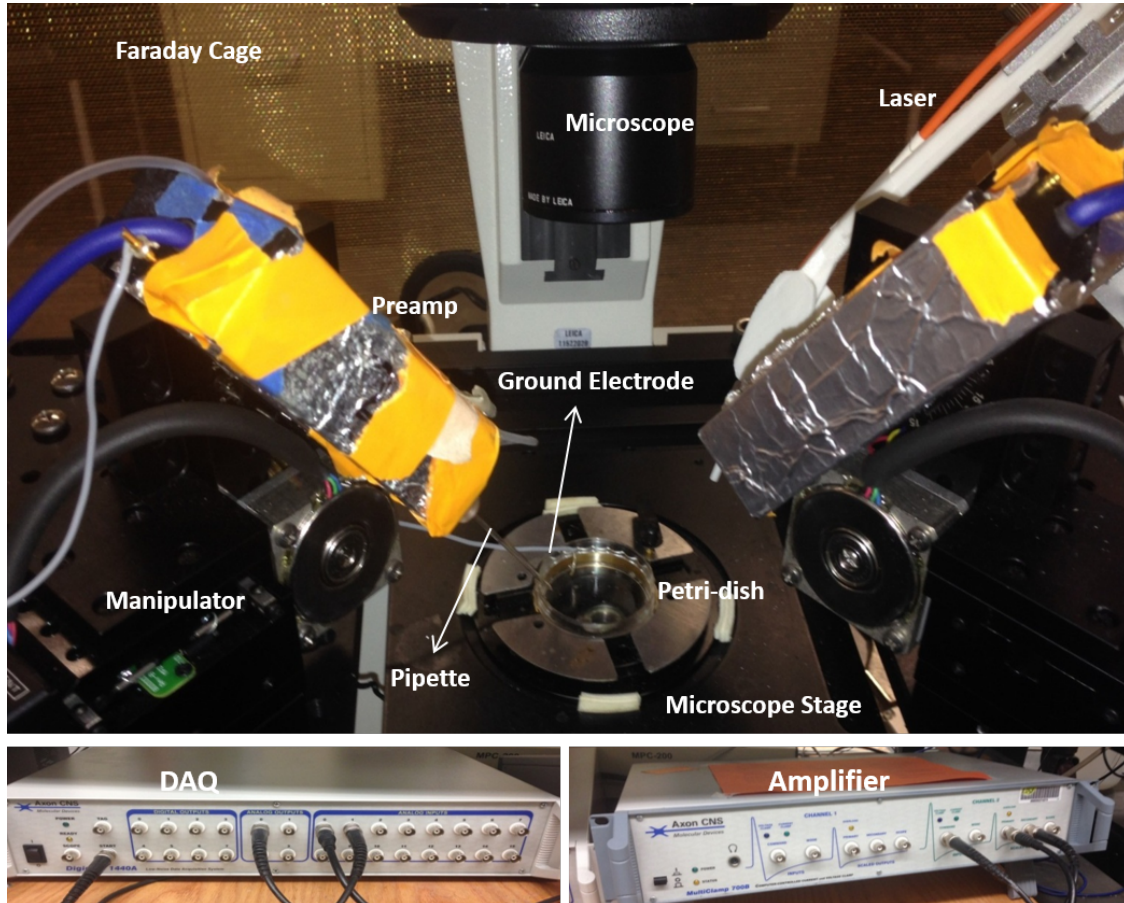
Figure 2.3: Digital micrograph of patch clamp setup showing its various components.

2.5 Cell Culture

2.5.1 Neonatal Cardiomyocytes Culture

2-3 day old Sprague Dawley rat pups (8-10) were decapitated and their hearts were removed. The hearts were transferred to ice cold PBS with 20 mM glucose. The atria were removed using small scissors to expose the ventricular cardiomyocytes. The ventricles were minced into small

12
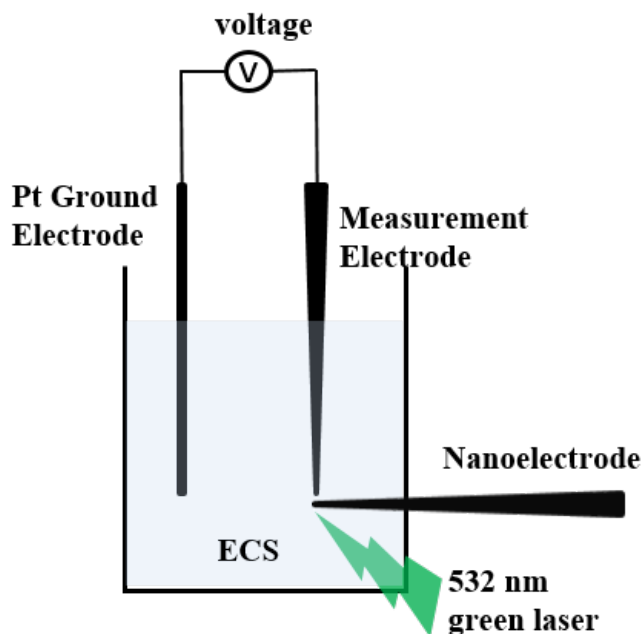
Figure 2.4: Schematic diagram of plasmonic measurement experiment in which the nanoelectrode was not part of the electrochemical cell circuit.

pieces and transferred into a 50 ml Falcon tube, and 7 ml of type-II collagenous solution was added to the tube. After that, the tube was heated in a water bath maintained at $37\,^{\circ}\mathrm{C}$ for 5-6 min with gentle shaking. The supernatant was transferred to another 50 ml Falcon tube. Next, 7 ml of the stop solution was added to the tube containing supernatant. The stop solution was M199 media with 5% FBS and 0.1% PenStrep. 7 ml of type-II collagenous solution was added into the first tube having the remaining undigested ventricular cardiomyocytes. The tube with the collagenous solution was again heated in a $37\,^{\circ}\mathrm{C}$ water bath for 5-6 min with gentle shaking. Then, the supernatant was transferred to the tube containing the earlier digested supernatant and stop solution mixture. 7 ml of stop solution was added to make the collagenous solution inactive. The procedure was repeated until cells were digested completely. The tubes containing digested cardiomyocytes were centrifuged at 3000 rpm for 2-3 minutes. The cell pellets were re-suspended into PBS and centrifuged again at 2500 rpm for 2-3 minutes. The pellets were suspended into 13 ml of day 1 medium - M199 containing 5% FBS, 10% horse serum and 0.1% PenStrep. The solution was incubated at $37\,^{\circ}\mathrm{C}$ with 5% CO_2 for 1 h.

13
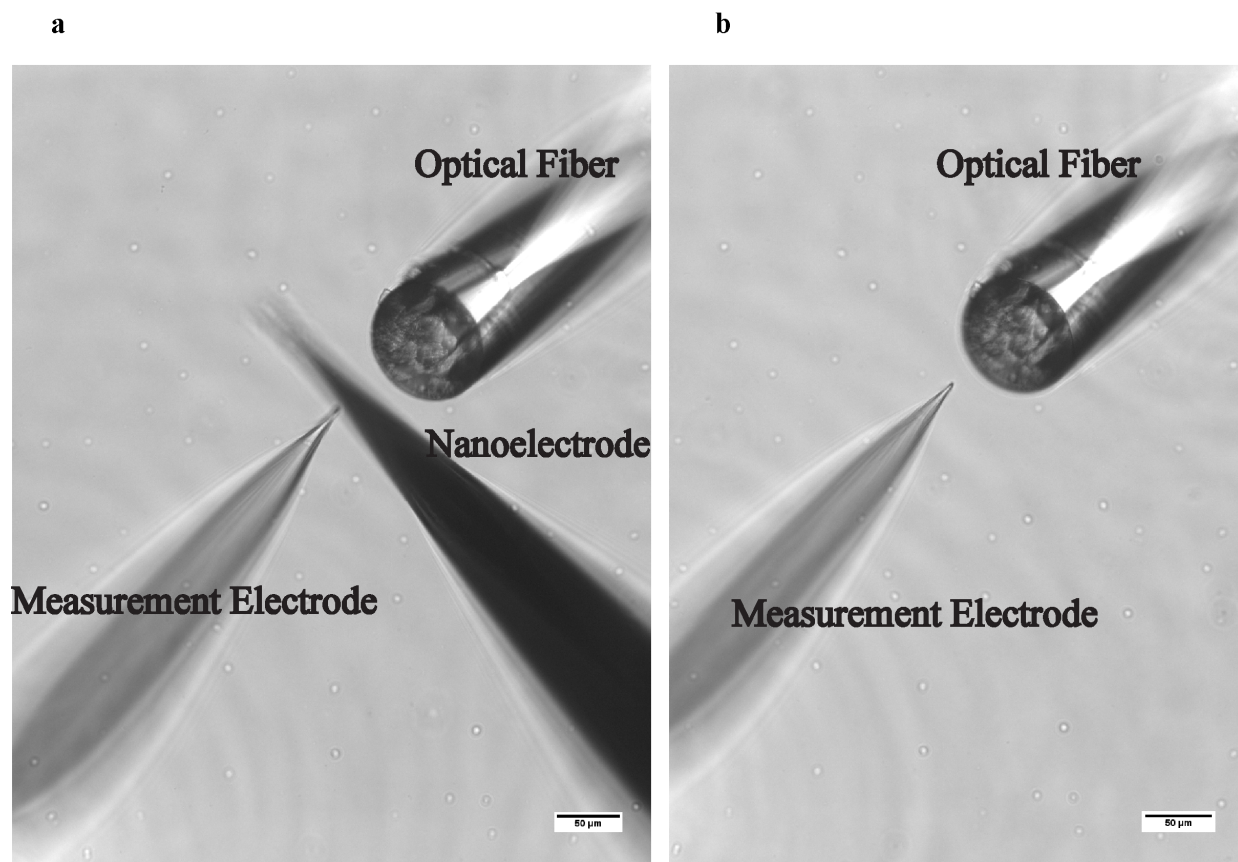
Figure 2.5: Digital micrographs were taken during the plasmonic temperature measurement at the surface of the nanoelectrode. (a) The digital micrograph of the plasmonic temperature measurement experiment showing the nanoelectrode, a patch pipette filled with extracellular solution, known as the measurement electrode, placed near the nanoelectrode surface; and a 50 μm inside diameter optical fiber used to focus a 532 nm green laser on the surface of the nanoelectrode (b) The control experiment showing the measurement electrode and a 50 μm inside diameter optical fiber (no nanoelectrode).

Next, the supernatant was diluted with day 1 medium and incubated in 35 mm laminin-coated petri dishes at $37\,^{\circ}$C with 5 % CO_2 for 24 h. On day 2, dishes were washed with PBS twice and the day 2 medium was used. The day 2 medium had the same composition as the day 1 medium except for the amount of FBS. It contained 1% FBS instead of 5% FBS. The medium was changed every 24-48 h. The cardiomyocytes showed spontaneous beating on day 3. These cells are good for patch clamp experiments at days 2 to 5 (Salameh and Dhein, 2005).

2.5.2 Differentiation of SH-SY5Y Neuroblastoma Cells

SH-SY5Y(ATCC® CRL-2266) neuroblastoma cell lines can be differentiated to neurons in presence of retinoic acid. The cells were initially cultured in a medium which is mixture of F12 & DMEM (1:1, v/v) containing 10% FBS and 1% PenStrep at $37\,°C$ with 5 % CO_2. The medium was changed every 4-7 days. After 80-90% confluence, trypsin was added to detach the cells. The cells in trypsin solution were incubated for 1-2 min. Then, an equal volume of medium, DMEM:F12 (1:1 v/v) with 10% FBS & 1% PenStrep, was added to neutralize the trypsin. The cells were centrifuged at 1500 rpm for 5 min. Next, the cell pellets were suspended in 90% FBS, 10% DMSO for long-term storage in 1.5 ml screw cap vials in a liquid nitrogen cylinder. For the subculture, cell pellets were suspended in medium, DMEM:F12 (1:1, v/v), 10% FBS, 1% PenStrep. After 48 h of plating, the medium was replaced with the Neurobasal medium containing supplements B27 and GlutaMAX. 10 μM all-trans-retinoic acid (ATRA) was added to this medium to promote neural differentiation. Along with promoting differentiation, the retinoic acid inhibits cell growth and proliferation as well. The medium was changed every 48 h (Kovalevich and Langford, 2013; Phlman et al., 1984).

2.6 Electrophysiology

All the physiological experiments were done using the whole cell configuration of the patch clamp technique, whose set-up is shown in Figure 2.3 (Multiclamp 700B amplifier and Digidata 1440A data acquisition system from Molecular Devices). For plasmonic stimulation, the nano-electrode was placed adjacent (within 2 μm) to the cell, while the cell was patched in whole-cell configuration using another microelectrode to measure the plasmonic responses. 532 nm green laser pulses were focused on the nanoelectrode using an optical fiber with 50 μm inside diameter. Figure 2.6 shows the micrographs of one such plasmonic stimulation experiment with an SH-SY5Y cell.

15
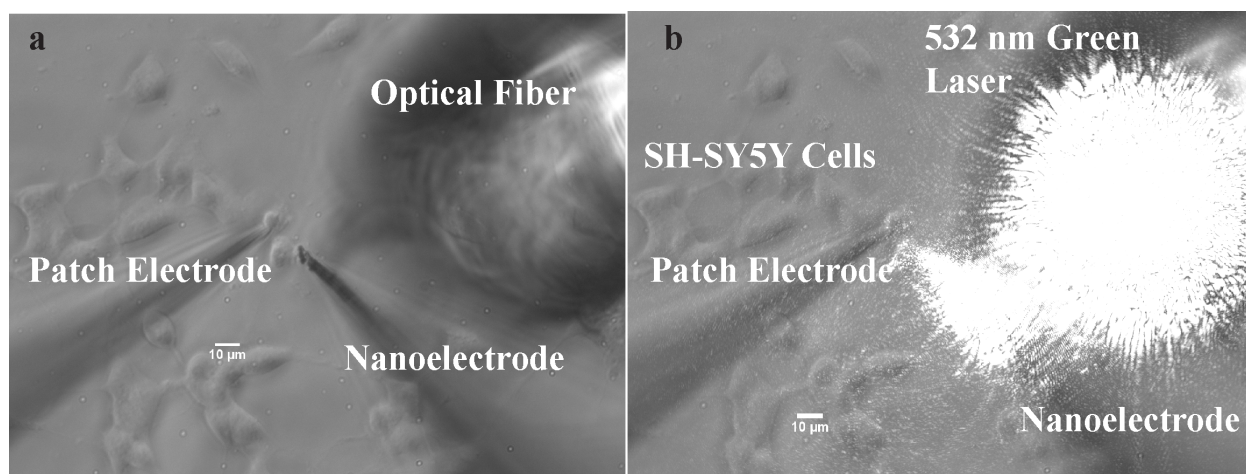
Figure 2.6: Digital micrographs showing the plasmonic set up in which our nanoelectrode was placed just next to an SH-SY5Y cell, and a recording microelectrode was used to patch the cell in whole-cell configuration. An optical fiber having an inside diameter of 50 μm was used to focus laser on the tip of the nanoelectrode (a) when laser was off and (b) when laser was on.

2.6.1 Neonatal Cardiomyocytes

Kang et al. (1995) studied the effects of fatty acids on various parameters of action potential generation for neonatal cardiomyocytes, like strength of depolarization current, cycle time and so on. We used their control current clamp experiment protocol to record action potentials from neonatal cardiomyocytes. The control experiments and plasmonic stimulation experiments were done at room temperature with no perfusion. The microelectrode resistance was 2.5-4.0 MΩ. The extracellular solution was 140 mM NaCl, 5 mM KCl, 1 mM $MgCl_2$, 2 mM $CaCl_2$, 10 mM HEPES at pH 7.4 maintained with NaOH. The intracellular solution used to fill the microelectrodes was 140 mM KCl, 2 mM $MgCl_2$, 1 mM $CaCl_2$, 5 mM MgATP, 10 mM NaCl, 10 mM HEPES, 10 mM EGTA, and pH 7.2 maintained with KOH.

2.6.2 SH-SY5Y Cells

Johansson (1994) recorded action potentials from differentiated SH-SY5Y human neuroblastoma cells. Tosetti et al. (1998) studied the effect cell differentiation on potassium currents and

16

its parameters by comparing differentiated and undifferentiated cell lines using whole-cell voltage clamp experiments. We recorded action potentials from undifferentiated and differentiated cells using the protocol of Tosetti et al. (1998) and also, recorded the plasmonic stimulation responses in the whole-cell configuration. The patch pipette had a resistance 4.5-7.5 MΩ. All the experiments were done at room temperature without perfusion. The extracellular solution contained 125 mM NaCl, 4 mM KCl, 2 mM $CaCl_2$, 1.2 mM $MgSO_4$, 10 mM glucose, 10 mM HEPES. The pH of the extracellular solution was maintained at 7.4 using NaOH. The intracellular microelectrode solution contained 140 mM KCl, 4 mM NaCl, 0.02 mM $CaCl_2$, 0.8 mM EGTA, 2 mM $MgCl_2$, 4 mM Mg-ATP, 10 mM HEPES. The pH of the intracellular solution was maintained at 7.2 using KOH.

17

3 RESULTS

3.1 Characterization of Gold Nanoparticles

3.1.1 UV-Vis Spectra

The strong absorption of a specific wavelength light by Au nanoparticles is responsible for the localized plasmon resonance phenomena. The ultraviolet-visible (UV/Vis) spectroscopy is used to quantify the absorbed and scattered light of a sample. A Perkin Elmer Lambda 35 UV/Vis spectrophotometer was used to obtain the UV/Vis spectra of our Au nanoparticles solution. Figure 3.1 shows the graph relating absorbance and wavelength for our gold nanoparticles solution. The peak absorbance around the wavelength 528 nm confirms the presence of Au nanoparticles.

3.1.2 Electron Microscopy Characterizations

An FEI Morgagni transmission electron microscope (TEM) was used to obtain images of gold nanoparticles. Figure 3.2 represents the two TEM images of gold nanoparticles: at a 100 nm scale bar and at a 20 nm scale bar. In addition to TEM, an Hitachi S-800 scanning electron microscope (SEM) was used to image the gold nanoparticles. Figure 3.3 shows the two SEM images of gold nanoparticles: at a 100 nm scale bar and at a 50 nm scale bar.

3.2 SEM Imaging of Nanoelectrode

SEM images of gold nanoparticles coated onto a micropipette were obtained using a Hitachi SU70 SEM. Figure 3.4 represents the SEM images of Au nanoparticles coated onto a micropipette
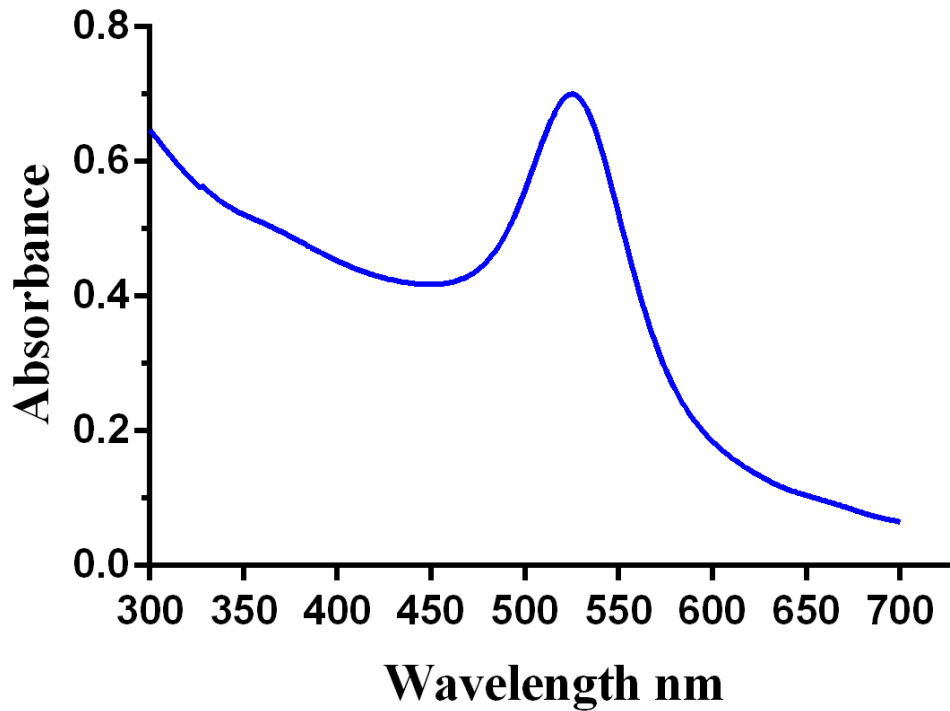
Figure 3.1: Absorbance spectrum of gold nanoparticles.

(10 μm, 1 μm, 500 nm and 300 nm scale bars). SEM images clearly show the uniform coating of gold nanoparticles onto glass micropipette.

3.3 Testing of Nano-electrode

Nanoelectrodes were tested using two methods before stimulation experiments with biological cells - Light-induced photocurrent method and fluorescence quenching.

3.3.1 Light-Induced Photocurrents

As reported by Lowe et al. (2003), we also observed photocurrents when our Au nanoparticles coated microelectrode was illuminated with a 100 mW 532 nm green laser with 0.1 M phos-

19
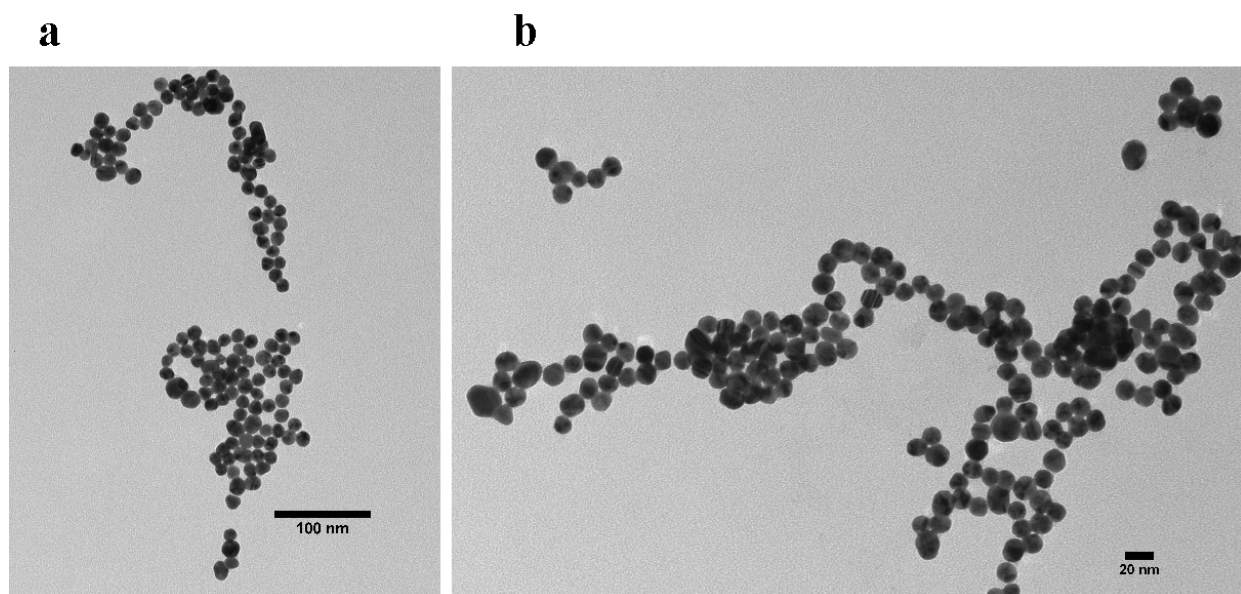
Figure 3.2: TEM images of gold nanoparticles: (a) a 100 nm scale bar and (b) a 20 nm scale bar.

phate buffer having 0.05 M EDTA as the electrolyte. Figure 3.5 shows measured photocurrents. When there were no nanoparticles coated on the microelectrode, no photocurrent was observed (figure 3.5). The photocurrents have a linear relationship with the applied voltage (Figure 3.7a)

Similar photocurrent jumps were observed when an extracellular solution having a composition of 140 mM NaCl, 5 mM KCl, 1 mM $MgCl_2$, 2 mM $CaCl_2$, 10 mM HEPES at pH 7.4 maintained with NaOH was used as the electrolyte instead of phosphate buffer. Figure 3.6 shows the measured photocurrent when the extracellular solution was used as the electrolyte. The control experiment was done with the micropipette not coated with gold nanoparticles. Like in phosphate buffer, photocurrents in ECS also have a linear relationship with the applied voltage (Figure 3.7b)

The photocurrents occur due to temperature rise the nanoelectrode-electrolyte interface by plasmon excitation of Au nanoparticles. Temperature rise at the interface leds to alteration of open circuit voltage of the nanoelectrode with respect to reference electrode, results in photocurrents (Lowe et al., 2003).

20
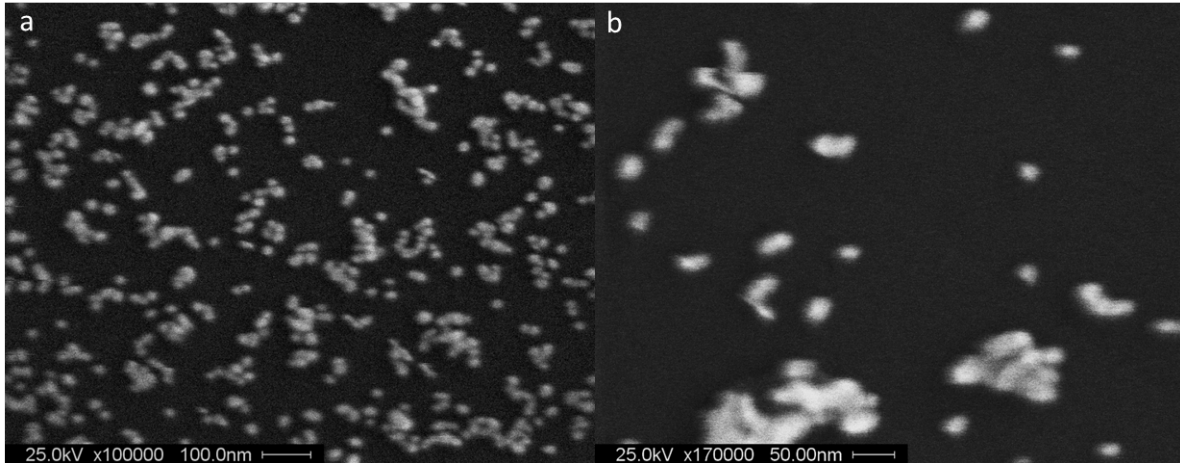
Figure 3.3: SEM images of gold nanoparticles: (a) a 100 nm scale bar and (b) a 50 nm scale bar.

3.3.2   Fluorescence Quenching

Metal nanoparticles like gold is known to strongly affect the emission spectra of fluorophores in their vicinity (Aslan et al., 2007; Aslan and Pérez-Luna, 2004). Nanoelectrodes were also tested for fluorescence quenching of FITC-labeled human serum albumin (HSA). FITC- labeled human serum albumin (HSA) was attached to the Au nanoparticles coated micropipette by incubating the nanoelectrode with a 10 μM solution of the fluorophore. A 488 nm laser source was used to excite FITC-HSA and the emission spectrum around wavelength of 520 nm was observed under an Olympus BX61W1 upright microscope. A fluorescence quenching was observed in the presence of Au nanoparticles (Figure 3.8b & c) in comparison to the control conditions (uncoated glass micropipette tips) (Figure 3.8a).

3.4   Plasmonic Temperature Measurements

3.4.1   Pipette Resistance Method

The indirect pipette resistance method used to measure plasmonic temperature measurement was adapted from Yao et al. (2009), measured temperature rise for the infrared stimulation of

21
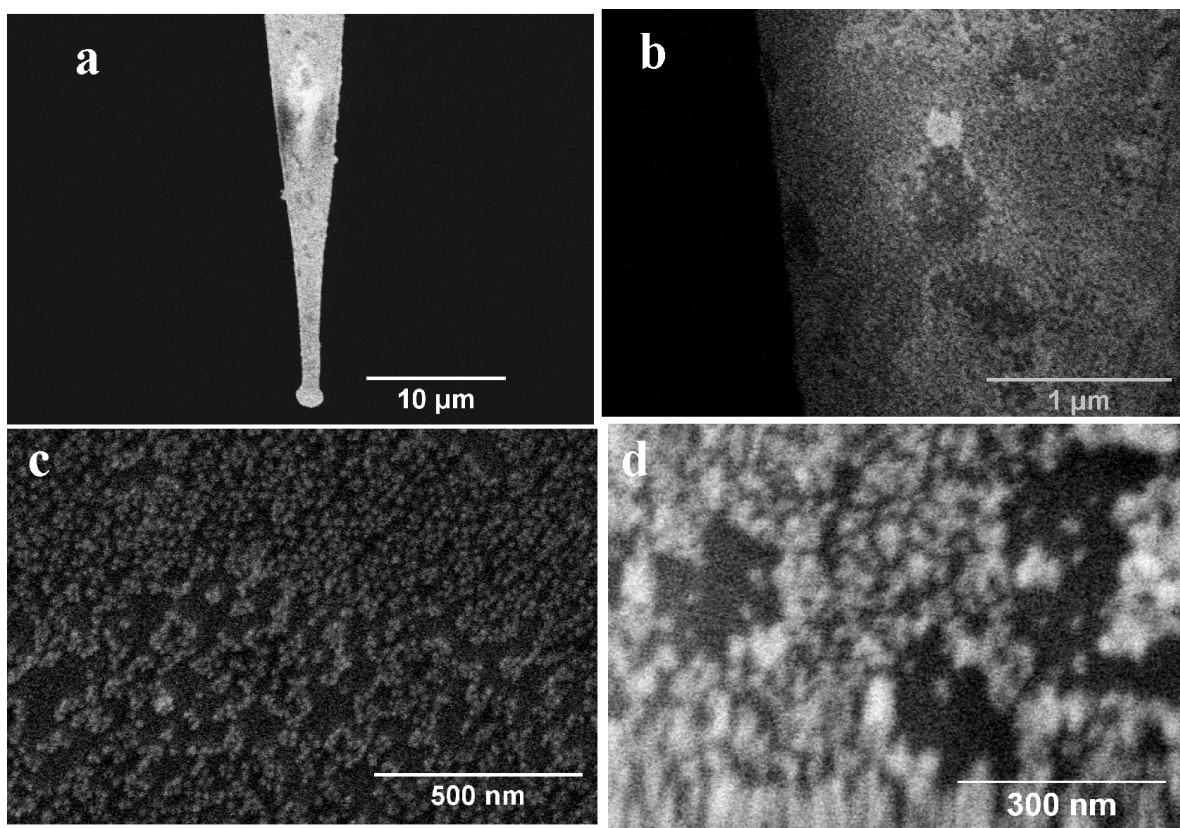
Figure 3.4: SEM images of nanoelectrode, micropipette coated with gold nanoparticles: (a) 10 μm scale bar, (b) 1 μm scale bar, (c) 500 nm scale bar, and (d) 300 nm scale bar.

biological cells (Shapiro et al., 2012). For calibration curve, the extracellular solution was heated to approximately 55 °C, then, allowed to cool down to room temperature. The resistance of a patch pipette filled with the same extracellular solution was recorded as temperature cooled down. Figure 3.9 represents the log (R) vs 1/temperature, fitted as a straight line, calibration curve. The blue curve was used for temperature calculations.

Figures 2.4 and 2.5 show the plasmonic temperature measurement setup where a patch pipette was placed just next to the nanoelectrode and a change in pipette resistance was measured when the laser was shined on the tip of the nanoelectrode. When 20 mV voltage pulses were applied to the patch pipette, there were extra instant jumps in current responses along on top of the voltage pulse response, as soon as the laser was turned on at maximum power (100 mW). These jumps go away when the laser was turned off (Figure 3.10). There were no current jumps, when the nanoelectrode
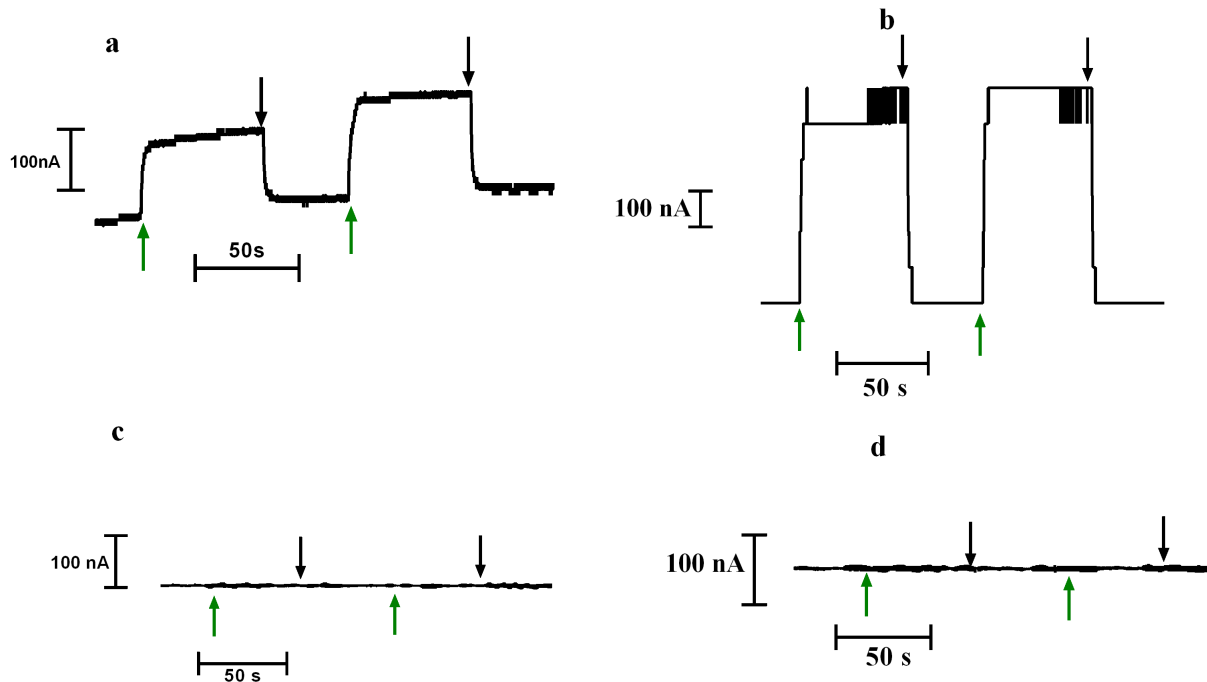
Figure 3.5: Photocurrents vs time in 0.1 M phosphate buffer having 0.05 M EDTA. (a) a microelectrode coated with gold nanoparticles when 0.3 V vs $Ag_{(s)}$/AgCl, reference electrode was applied (b) a microelectrode coated with gold nanoparticles when 0.9 V vs $Ag_{(s)}$/AgCl, reference electrode was applied (c) a microelectrode with no gold nanoparticles coating when 0.3 V vs $Ag_{(s)}$/AgCl, reference electrode was applied (d) a microelectrode with no gold nanoparticles coating when 0.9 V vs $Ag_{(s)}$/AgCl, reference electrode was applied. The green upward arrows represents when laser was turned on and black downward arrows represent when laser was turned off.

was not present (Figure 3.10). These current jumps correspond to $33\,°C$ temperature rise from the room temperature ($22\,°C$ to $55\,°C$).

As a control measurement, the temperature rise was studied as a function of laser power. The plasmonic temperature increases linearly with the laser power (Figures 3.11a & c) and decreases exponentially with the distance away from the nanoelectrode (Figure 3.11b).

3.4.2 Infrared Thermography

The change in temperature of 0.3 to $0.4\,°C$ was measured at the nanoelectrode-electrolyte interface using infrared thermal camera (Figure 3.12).

23
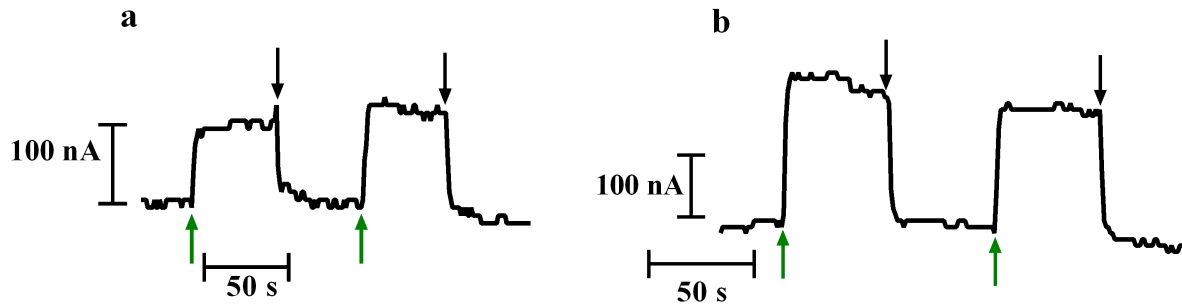
Figure 3.6: Photocurrent measurements when extracellular solution was used as the electrolyte. (a) A 0.6 V voltage vs Ag(s)/AgCl, reference electrode was applied. (b) A 0.9 V voltage vs Ag(s)/AgCl, reference electrode was applied.

3.5   Plasmonic Physiological Responses

All the plasmonic stimulation experiments were done by using our patch clamp set up - Multiclamp 700 (Figures 2.3, 2.6). Cells were patched by forming the gigaseal in voltage clamp mode and whole cell patch clamp configuration was achieved by applying the slight negative pressure with the help of 1 ml syringe. After that, all recordings will be done under current clamp mode.

3.5.1   Neural Activation

When SH-SY5Y cells were stimulated with a 10 ms or longer laser pulse, jumps in membrane potential - plasmonic jumps were observed. These jumps in potential change magnitude, relative to the holding potential of the cell, were positive when the cell was at holding potentials -30 mV or less. As the holding potential approaches zero, the magnitude of the plasmonic jumps decreased and become negative as the holding potential went to more positive. Figure 3.13a shows one of these recordings from a differentiated SH-SY5Y cell. Cells were firing action potential both, before and after, the plasmonic stimulation portion of the experiment (Figure 3.14). For control experiments (laser stimulation alone - without nanoelectrode), no cellular response was observed (Figure 3.13b)

24
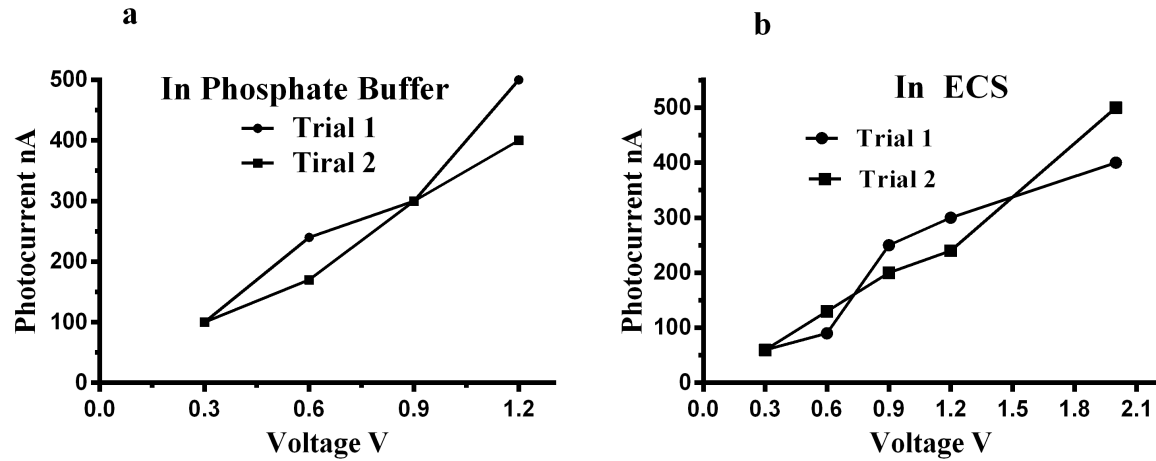
Figure 3.7: Photocurrents increase with applied voltage for both electrolytes: (a) 0.1 M phosphate buffer/0.05 EDTA and (b) NaCl (125 mM) based extracellular solution.

Positive plasmonic jumps indicate the depolarization due to opening of sodium channels and negative plasmonic jumps indicate the repolarization because of the opening of potassium channels. Figure 3.14 shows the action potential recordings before and after the plasmonic stimulation from the same cell whose plasmonic jumps are shown in Figure 3.13. Figure 3.15 provides the data showing the relations between plasmonic jumps and the holding potential for six different neurons. All the cells show the same trend. It has also been observed that magnitude of plasmonic jumps increases as pulse timing increases at a particular laser power but plasmonic jumps rise at a slow rate (Figure 3.16).

Plasmonic jumps also increases with increase in laser power. Figure 3.17 shows change in membrane potential at different laser powers (20-100 mW). Experiments were carried out with rat neonatal cardiomyocytes as well and similar plasmonic jumps were observed, increases with increases in laser power (Figure 3.18).

For laser pulse widths of 1-5 ms, action potentials were recorded from the cells. Figure 3.19 shows action potential recordings for a representative SH-SY5Y cell when the nanoelectrode was illuminated with a 1 ms 532 nm green laser pulse with 100 mw power. Figure 3.20 shows these op-

tically stimulated action potential recordings from six different cells. To induce optical responses, we found that the laser power should be in the 60 mW - 120 mW range. At lower powers, there was generally no response recorded. Like for plasmonic jumps experiments, action potentials were recorded, prior and subsequent, to the optical stimulations in response to electrical current pulses (Figure 3.21). Following stimulation the resting potential slowly returns to pre-stimulus over a time span of seconds and up to a minute. (Carvalho-de Souza et al., 2015) also reported the similar observations for stimulation of dorsal root ganglion (DRG) neurons using functionalized gold nanoparticle attached to cell membrane. They have attributed it to transient membrane alteration due to optical stimulation.

3.5.2 Neural Inhibition

When optical laser pulses were superimposed on electrically stimulated action potential responses, while recording action potentials in standard current clamp experiments, a decreases in magnitude of the action potentials were observed. Action potentials were recorded before and after the optical stimulation experiments (Figure 3.22). As laser power increases, the inhibition become more prominent (Figure 3.23). Typically in an action potential, depolarization happens predominantly because of Na^+ ion exchange and repolarization happens mainly because of K^+ ion exchange. Different data analysis were carried out with respect to laser power for depolarization and repolarization phases of the action potentials. Figure 3.24 shows the various data analyses carried out for inhibition experiments with respect to laser power: action potential peaks (AP peaks), up-slope of the AP (rate of membrane potential rise from holding potential to peak value - rate of depolarization), difference between the initial peak value and first minimum of the action potential (AP Peak - Base), base value (first minimum after peak value) and the down-slope of the AP (rate of membrane potential fall from the peak value to base value - rate of repolarization).

The AP peak value decreased as laser power increased as shown in Figure 3.25. The rate of membrane potential rise from holding potential to peak value - up-slope, i.e., the depolarization

26

rate, remained unaffected by the laser power (Figure 3.26). The up-slope values were normalized by dividing each value with initial value of the up-slope for electrical action potential stimulation before the optical stimulation experiment. The normalized upslope also has the same trend as absolute values, i.e., there was hardly any change with the laser power (Figure 3.27).

The minimum after the AP peak, i.e., the base value did not change with increases in laser power (Figure 3.31). The differences between the peak & base values decreased with laser power (Figure 3.28).

The rate of membrane potential fall from peak value to the first minima after the peak - down-slope, i.e., the depolarization rate, decreased with increased laser power (Figure 3.29). Like up-slope, the down-slope values were normalized by dividing each value with the initial value of the down-slope for electrical action potential stimulation before the optical stimulation experiment. The normalized downslope also had the same trend as absolute values, i.e., decreased with the laser power as shown in Figure 3.30.

It can be noted that up-slope (depolarization rate) was unaffected by laser power while the down-slope (repolarization) decreased with laser power. As depolarization is mostly governed by exchange of Na^+ ions and repolarization is governed by exchange of K^+ ions, it is possible that during inhibition, the rate of K^+ ion transfer was affected more than the rate of Na^+ ion transfer. Since inhibition is largely governed by potassium channels. It has been reported in earlier studies that temperature sensitive potassium channels are involved in inhibition. For example, Yoo et al. (2014) reported significant decrease in neural activity in response to Au-nanorods activated with an infrared laser due to the responses of heat-sensitive TREK-1 channels.

Another set of experiments were conducted where the laser pulse led the electric current pulse by a few milliseconds. Figure 3.32 shows one such representative SH-SY5Y cell. The inhibition increases as laser pulse lead time increased.

27

To confirm the generalization of eliciting inhibition phenomena with visible light laser stimulation, experiments were conducted with spontaneous beating neonatal cardiomyocytes from rats. Like SH-SY5Y cells, the inhibition of action potential magnitude was observed for the neonatal rat cardiomyocytes. A decrease in action potential magnitudes became more significant at higher laser power levels, as shown in figure 3.33.

Both activation - optical stimulation alone and inhibition - optical stimulation in combination with electrical stimulation, were recorded from the same cells. Figure 3.34 shows a representative SH-SY5Y cell.
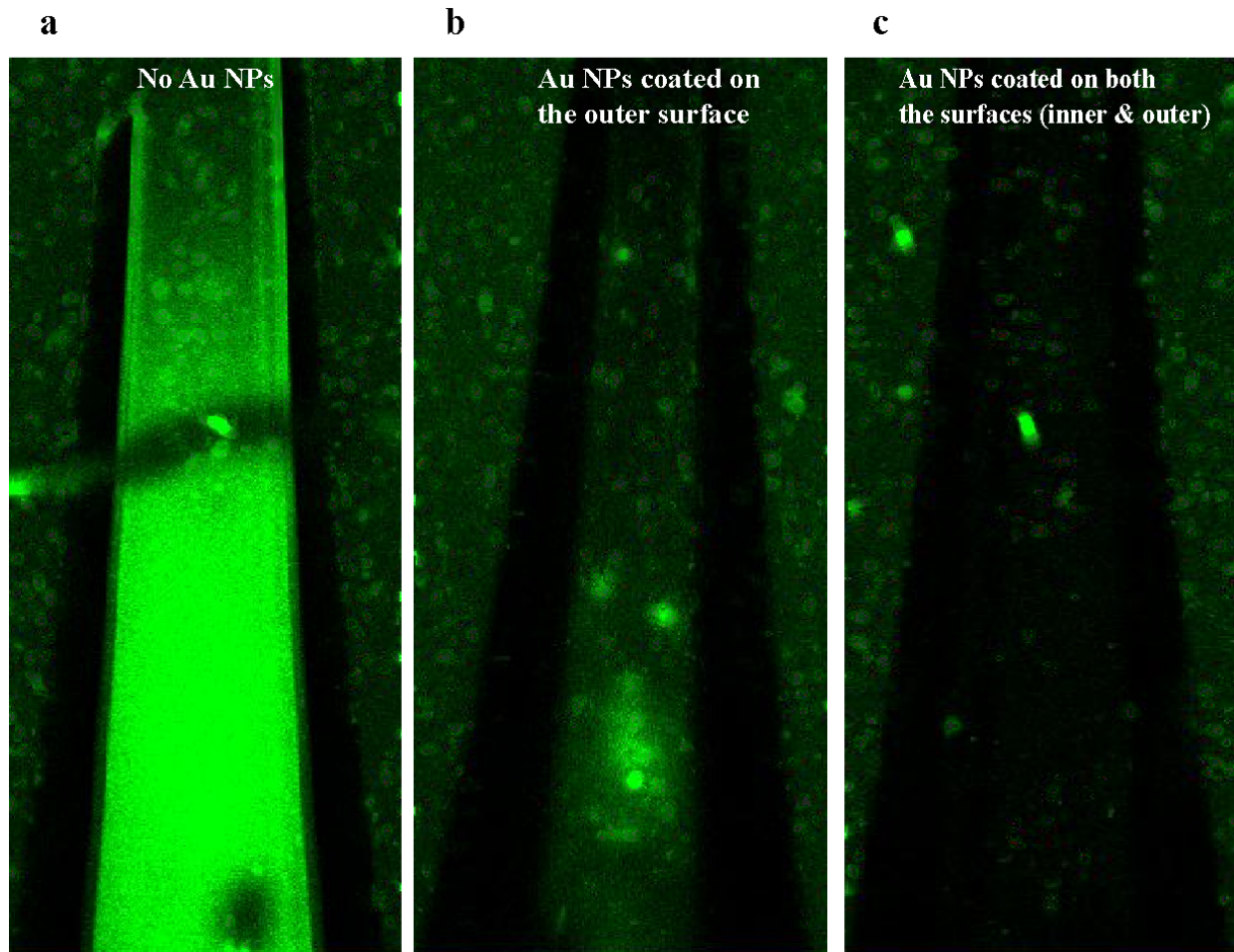
Figure 3.8: Digital micrographs of fluorescence emission of FITC-labeled human serum albumin (FITC-HSA) on glass micropipette tips. (a) uncoated tip (b) tip coated with Au nanoparticles outside and (c) tip coated both inside and outside. A 488 nm laser source was used to excite FITC-HSA and the emission spectrum around wavelength of 520 nm was observed under an Olympus BX61W1 upright microscope.
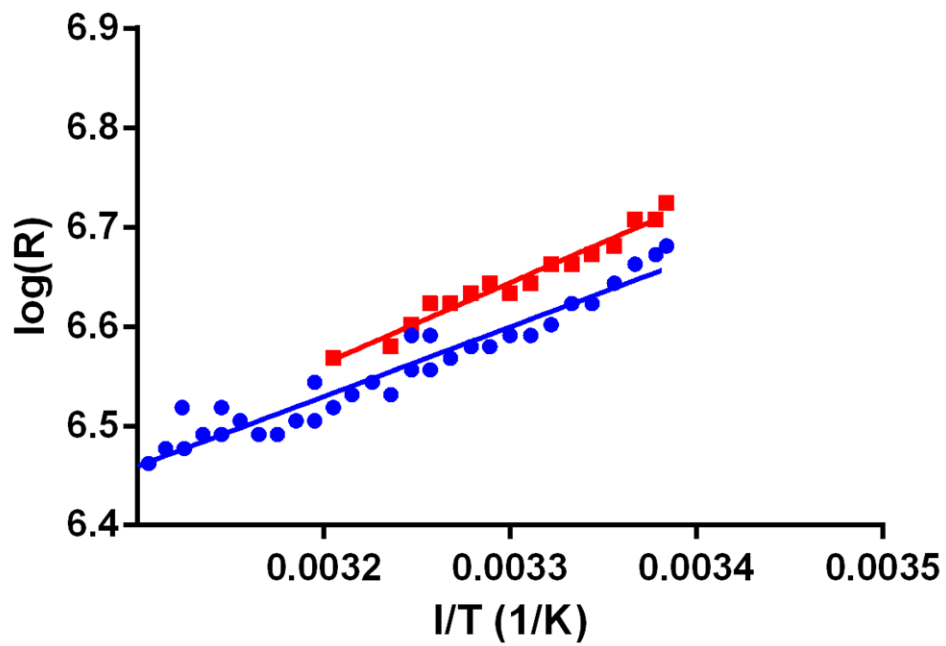
Figure 3.9: Micropipette resistance versus temperature calibration curve. The figure shows curve from two trials. Blue data points and line were used for temperature calculations because it has more data points.
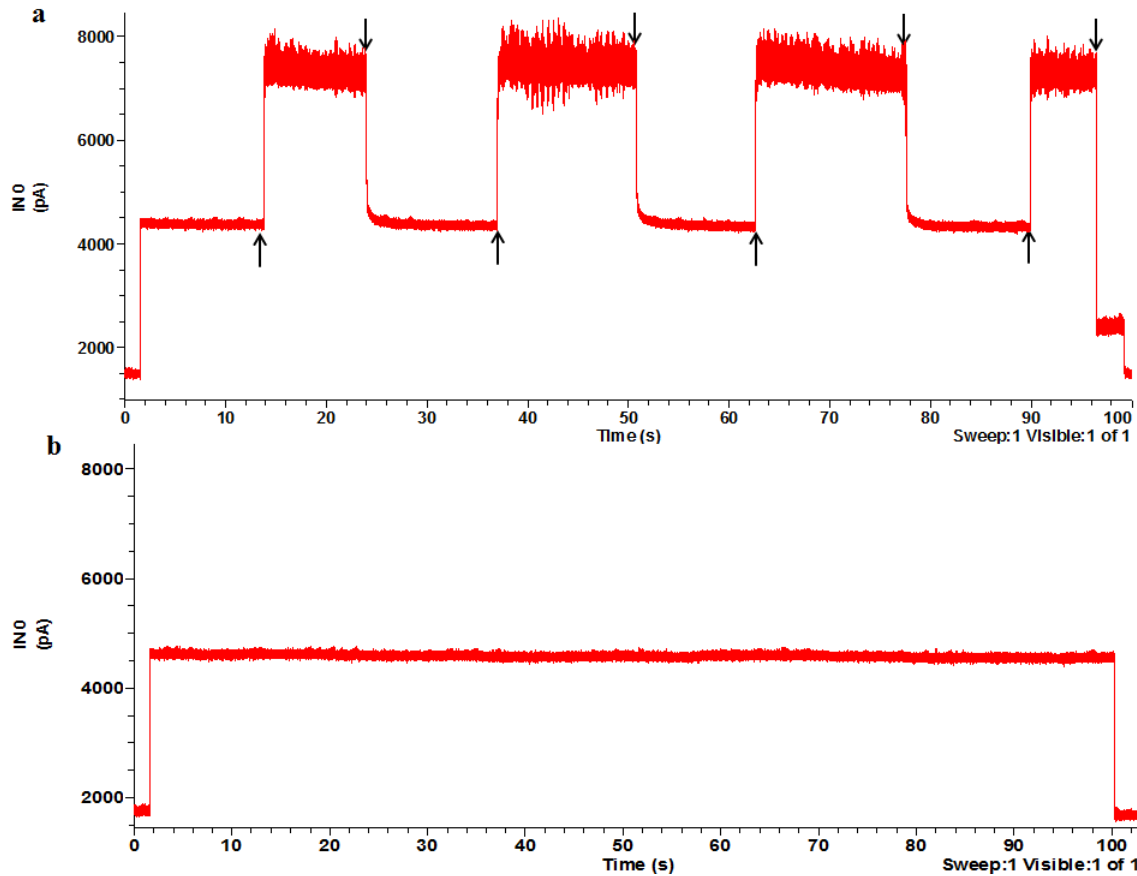
Figure 3.10: Current vs time curves in response to a 20 mV electrical pulse. (a) when the Au nanoelectrode was present, instant jumps in current were observed as soon as the laser (100 mW, 532 nm green laser) was turned on (upward arrows). These jumps are due to plasmonic heating and correspond to $33\,°C$ temperature rise from room temperature to approximately $55\,°C$. (b) There were no jumps when the nanoelectrode was not there. Downward arrows designate when the laser was turned off.

31
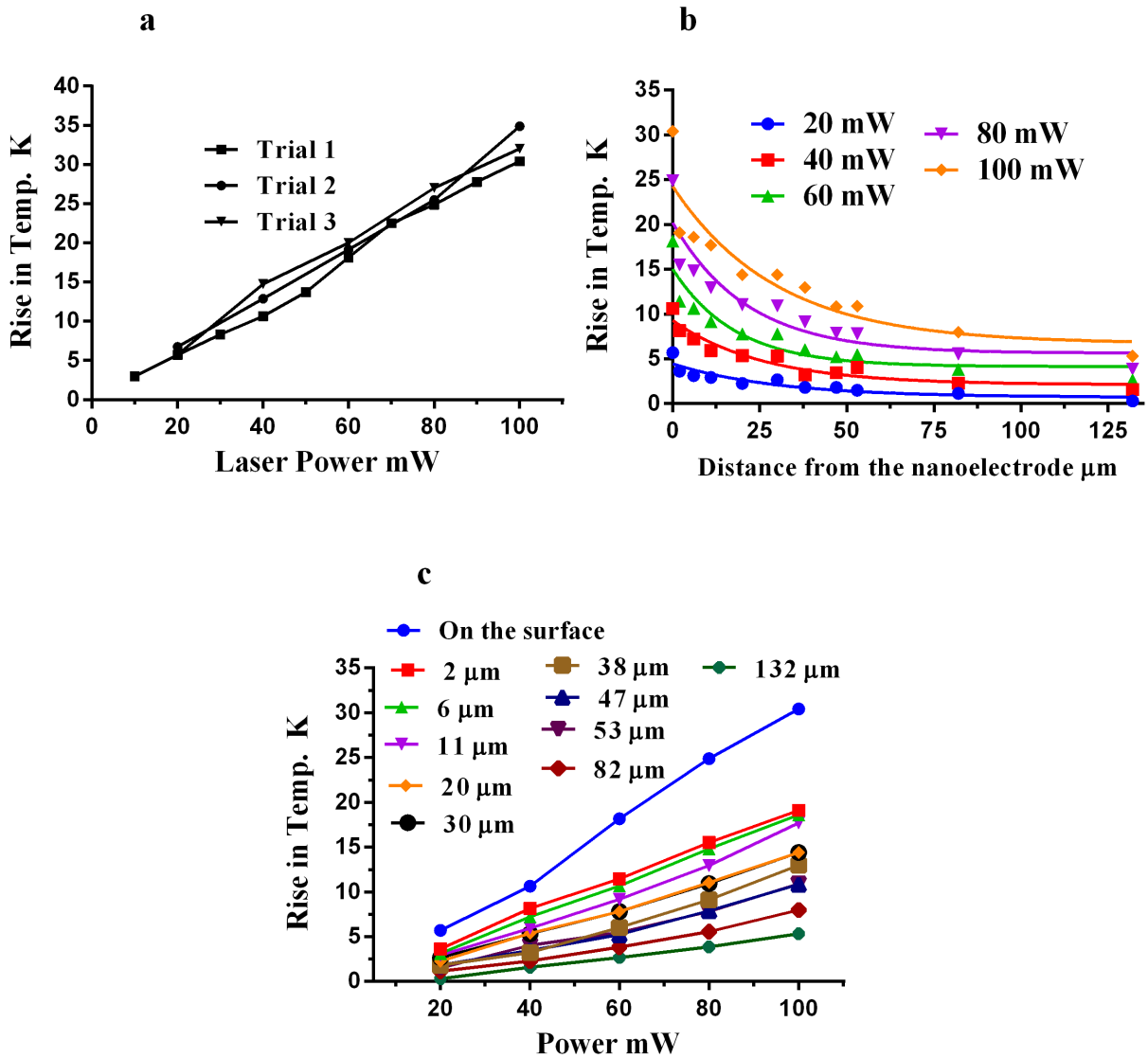
Figure 3.11: Plasmonic temperature measurements using pipette resistance method. (a) Laser power vs plasmonic temperature rise on the surface of the nanoelectrode (Three trials). As laser power increases, temperature-rise also increased, approximately linearly. (b) Plasmonic temperature rise vs distance from the nanoelectrode at various laser powers. The temperature rise decreases exponentially with distance. (c) Like on the surface of the nanoelectrode, temperature rise increases linearly with laser power at different distances away from the nanoelectrode.
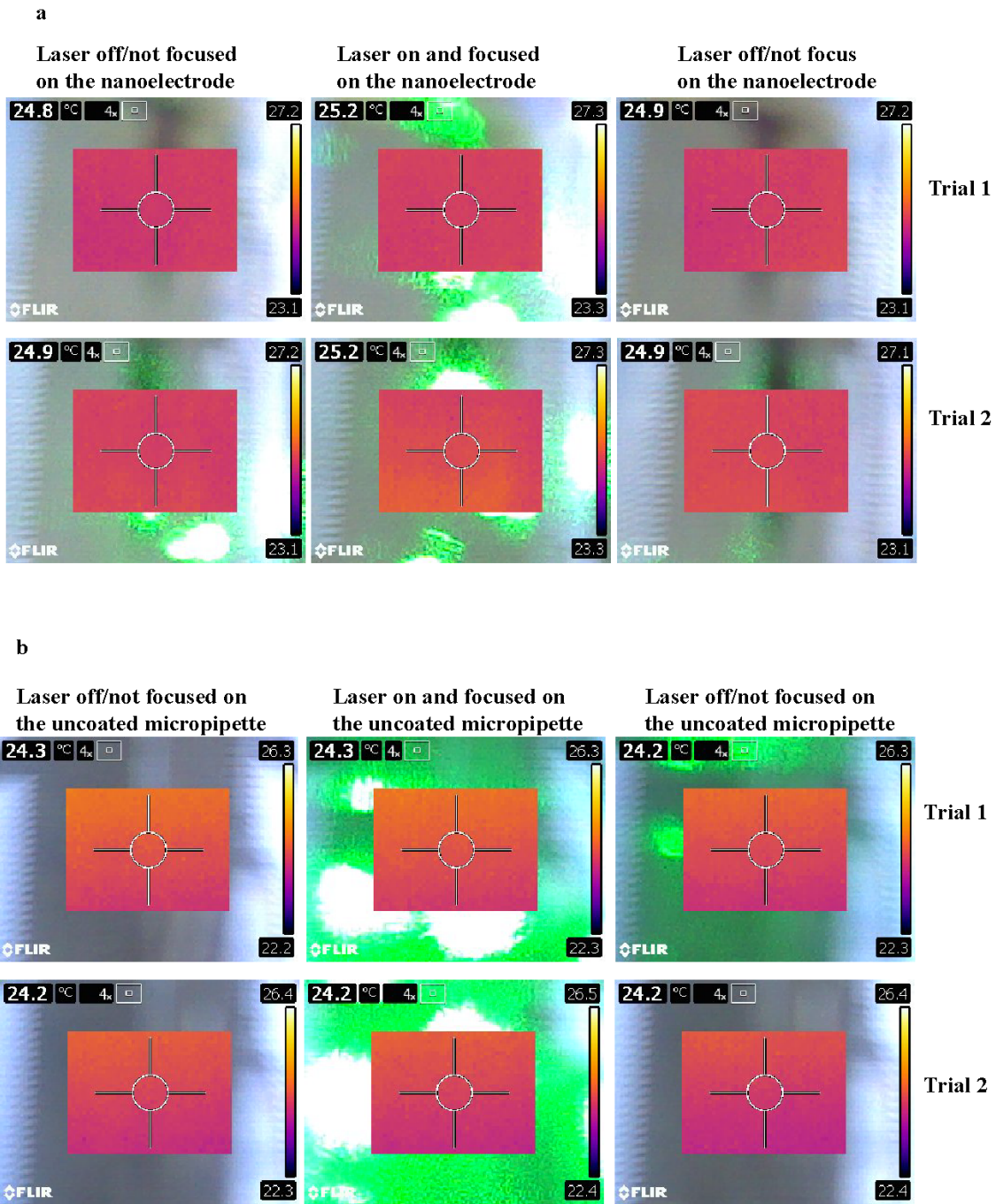
Figure 3.12: Infrared thermograms of glass micropipettes. (a) nanoelectrode - micropipette coated with Au nanoparticles and (b) control - uncoated micropipettes. Laser was either off or not focused on the tip of the micropipette (left), laser was switched on and focused on the tip of the micropipette tip (middle) and finally, laser was turned off again or not focused on the tip of the micropipette. The shadow in the background shows the micropipette.

33
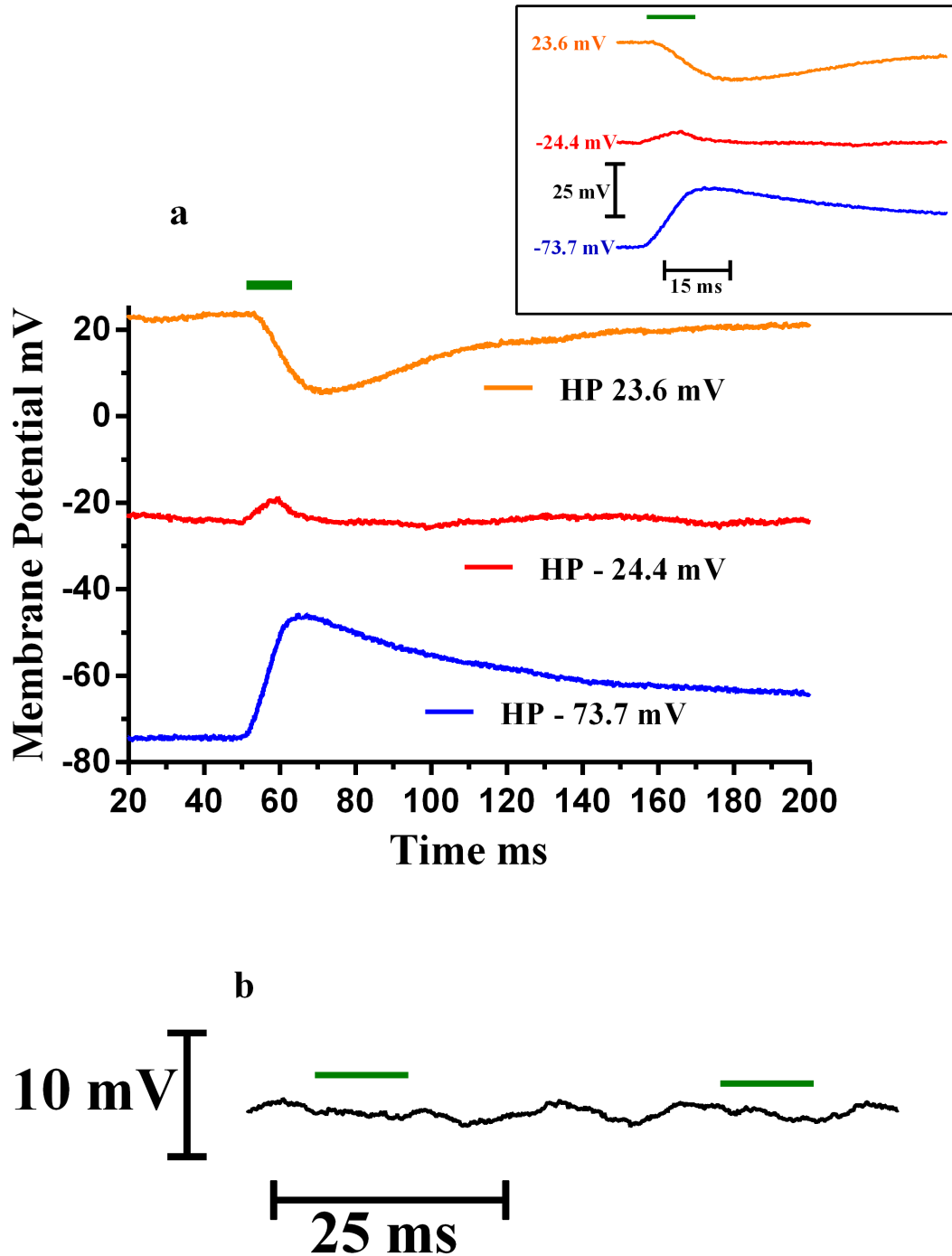
Figure 3.13: Plasmonic jumps for a representative SH-SY5Y cell. (a) Change in cell potential (plasmonic jumps) at different holding potentials during plasmonic stimulation, i.e. a 10 ms pulse having a power of 100 mW, was shined onto the nanoelectrode. The figure shows plasmonic jumps at three holding potentials: -73.7 mV, -24.4 mV and 23.6. The inset shows the onset response in more detail (faster time scale). (b) When optical stimulation experiments were done with laser along, without nanoelectrodes, no/little response was observed. Figure shows a SH-SY5Y cell with holding potential = -53.9 mV. The green bar represents the laser pulse timing.
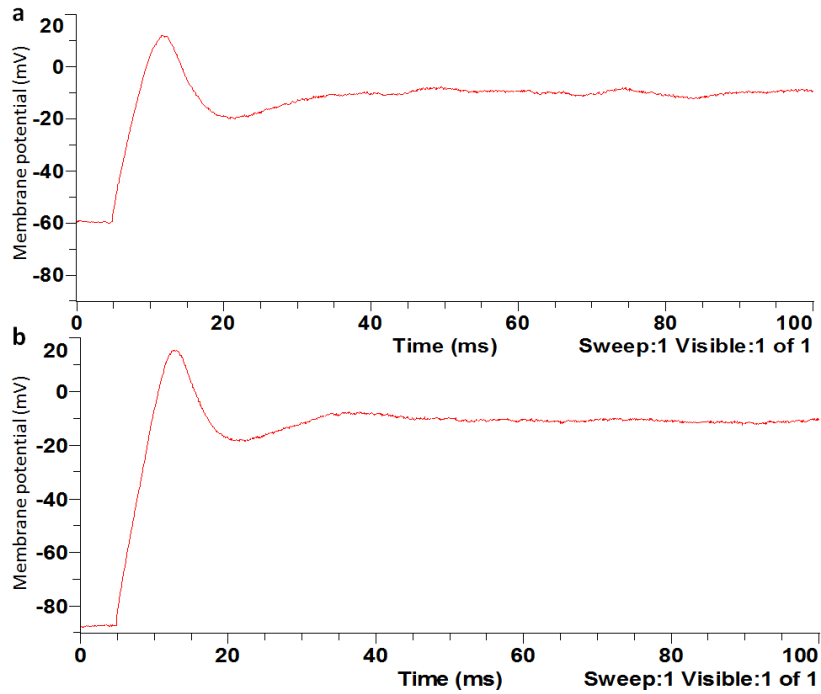
Figure 3.14: Action potentials recorded using standard whole cell current clamp procedure; (a) before plasmonic stimulation experiment and (b) after plasmonic stimulation experiment. It indicates that plasmonic stimulation is not doing any thermal damage to the cell, so, the neuron is otherwise healthy.
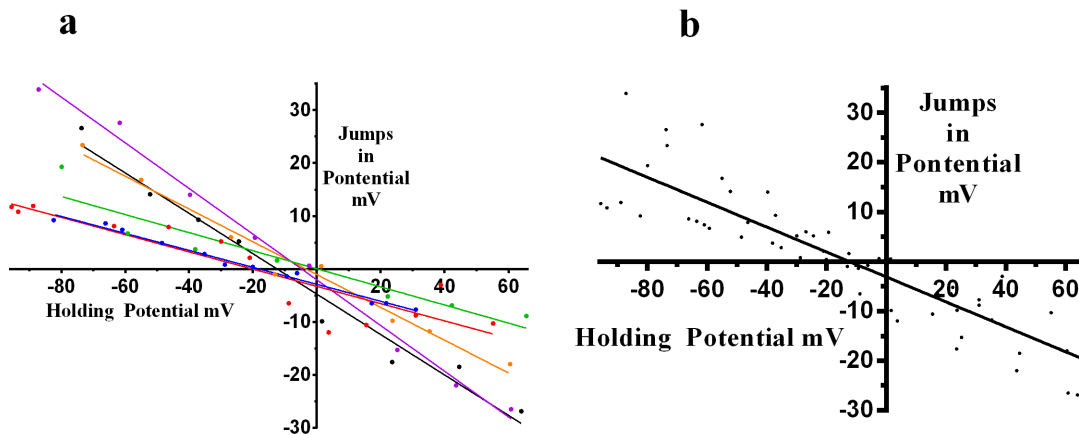
Figure 3.15: Plasmonic jumps versus membrane potential. (a) Plasmonic jumps versus holding potential graph for six different cells. Each cell is represented by different color data points and line. All show the same trend, i.e., as holding potential goes from negative to positive, plasmonic jumps go from positive to negative. (b) The average linear regression curve for holding potential versus jumps when cells were stimulated with 10 ms, 100 mW laser pulses.
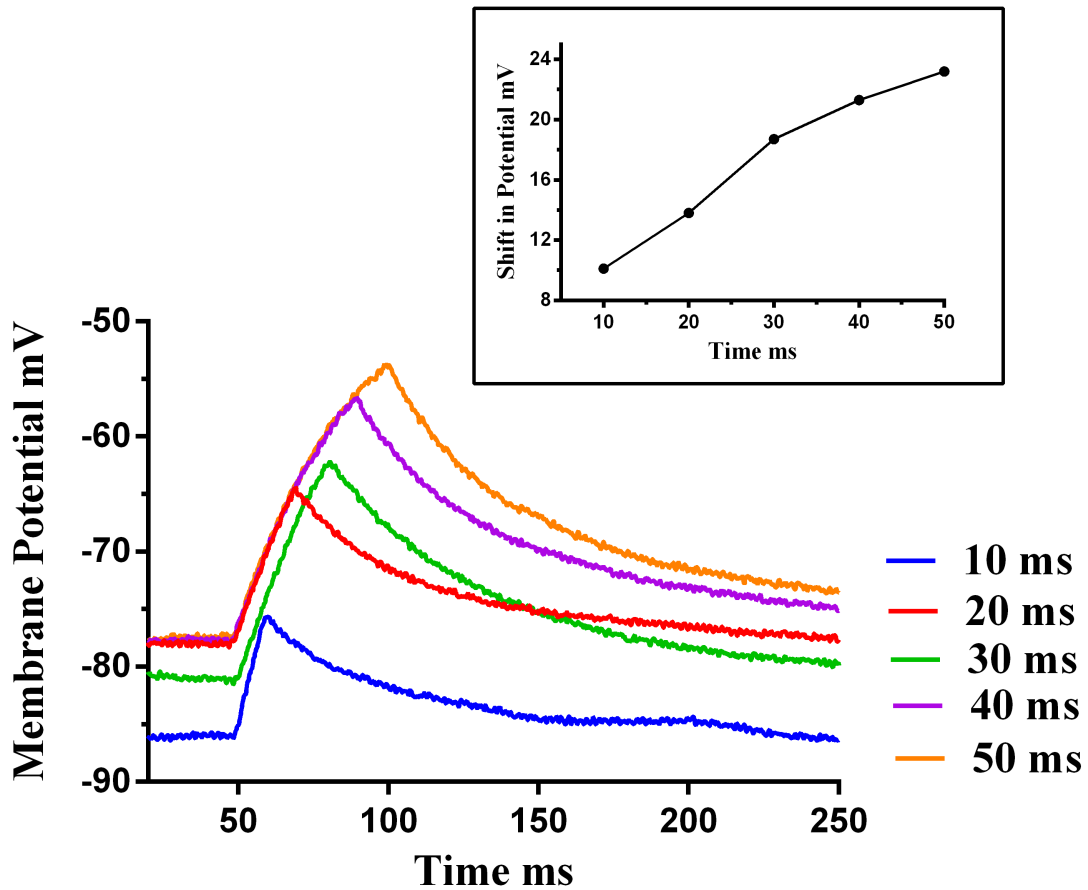
Figure 3.16: Plasmonic jumps of a representative SH-SY5Y cell at different pulse timings (10-50 ms) at 100 mW laser power. Plasmonic jumps increases in magnitude with pulse timing (inset) but the rate of rise slows down.
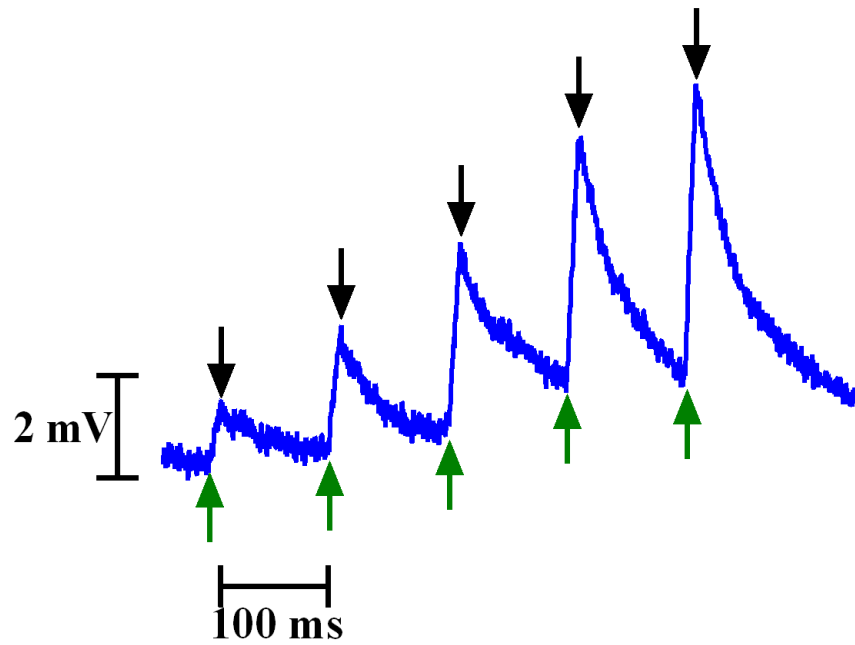
Figure 3.17: Plasmonic jumps of SH-SY5Y cells for 10 ms pulses at different laser powers; 20 mW, 40 mW, 60 mW, 80 mW and 100 mW (holding potential = -77.8 mV). The plasmonic jumps become more prominent at higher laser powers.
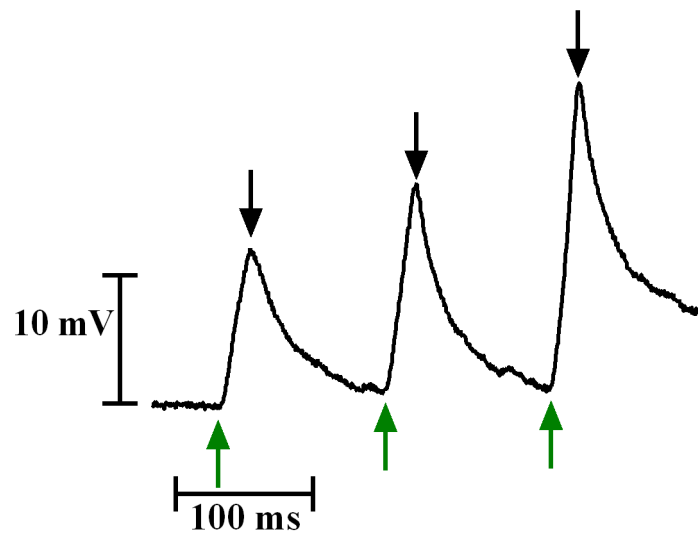
Figure 3.18: Shift in membrane potential for a representative neonatal cardiomyocyte at three different laser powers; 60 mW, 80 mW, 100 mW for 10 ms laser pulse timing.
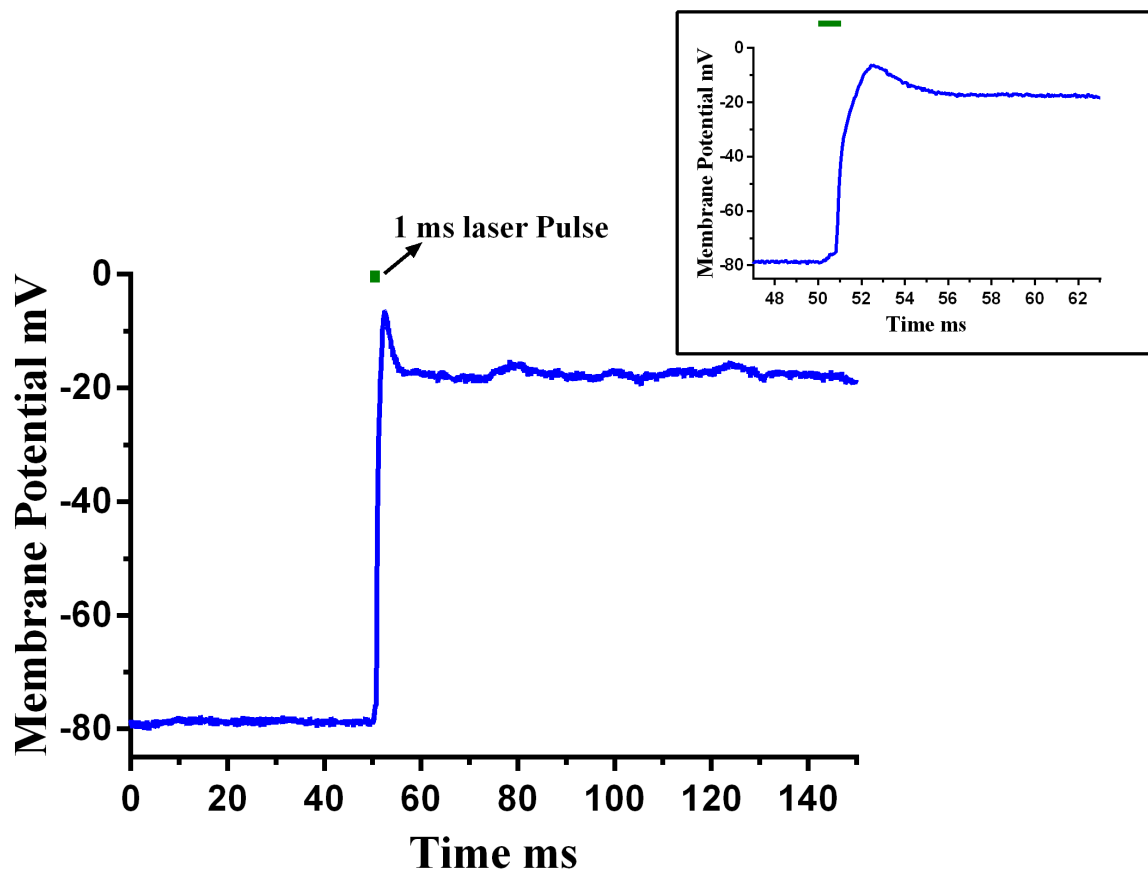
Figure 3.19: A representative action potential recorded from an SH-SY5Y cell for a 1 ms laser pulse at 100 mW laser power. For 1-5 ms laser pulses (100-120 mW laser power), action potentials were recorded from the SH-SY5Y neural cells. The inset shows the zoomed portion of the onset response for the same
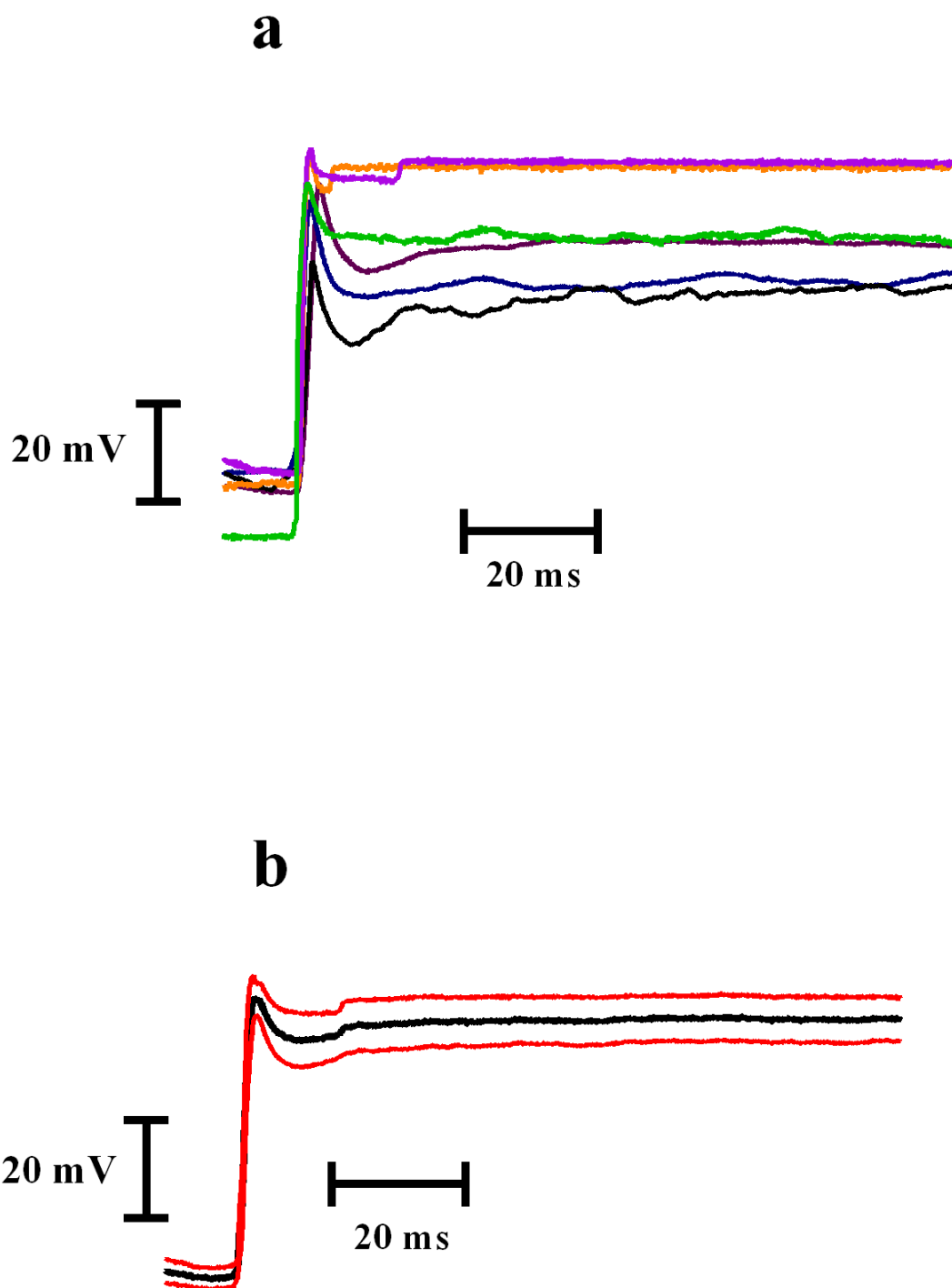
Figure 3.20: Optical action potentials. (a) Action potentials recorded, in response to the optical stimulation from six different neural cells, each a different color. (b) The mean curve of optically stimulated action potentials (N=6). Black curve shows the mean values and red curves show the sem values. All the experiments were done in whole current clamp mode using an electrophysio-logical patch clamp system.
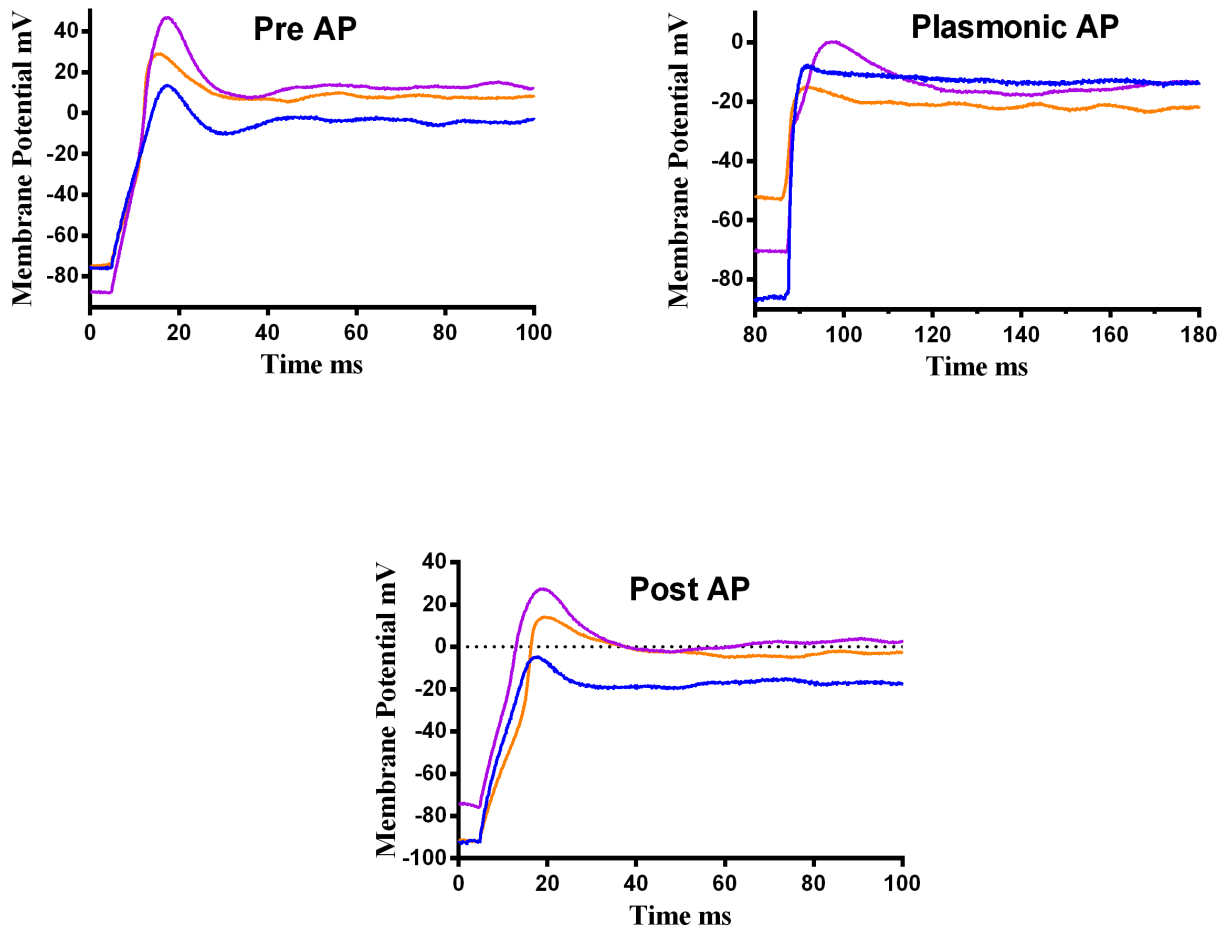
Figure 3.21: Electrically stimulated action potentials (pre AP & post AP) were recorded before and after the optical stimulation recordings (plasmonic AP). The figure shows three different such SH-SY5Y cells.
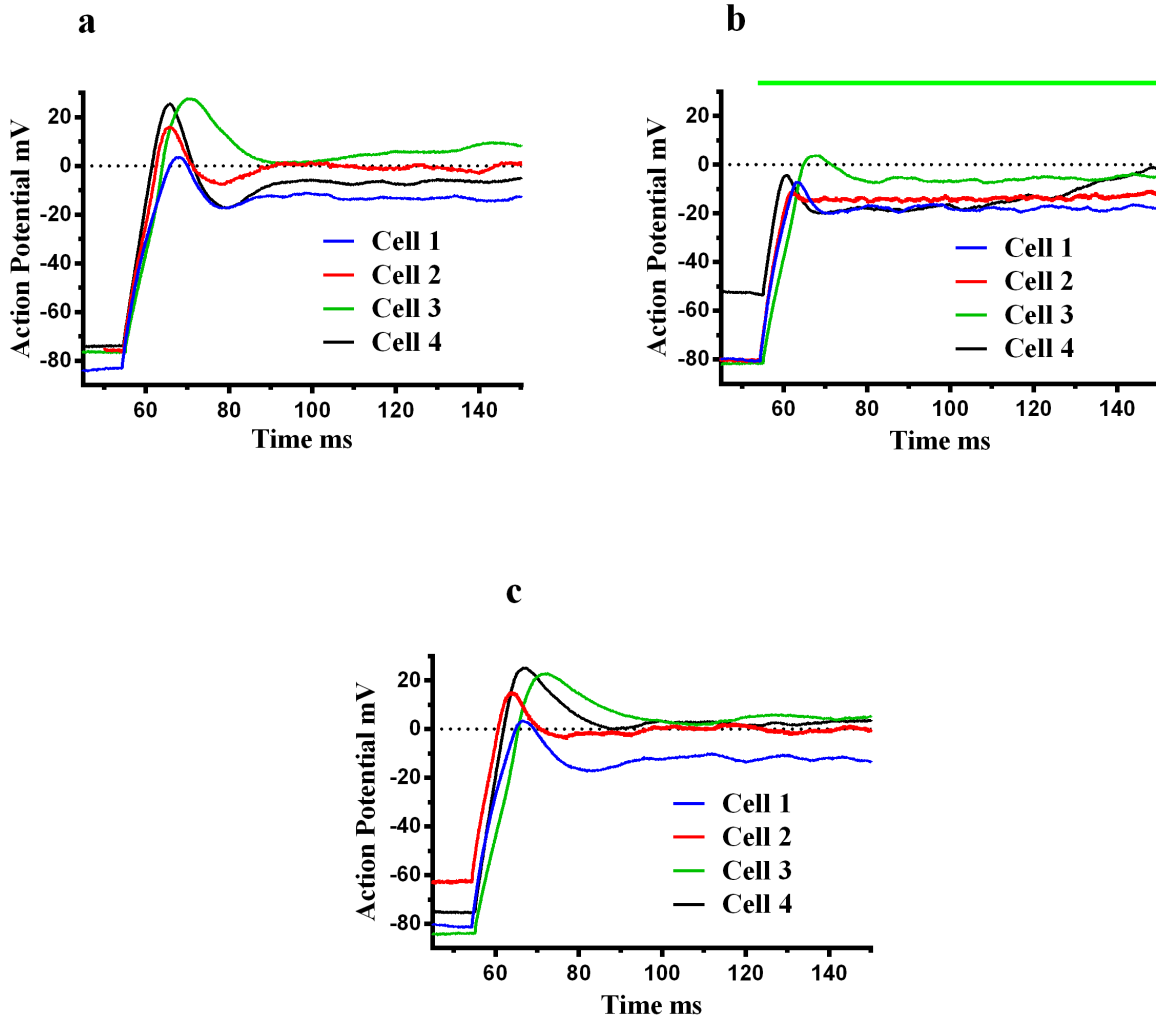
Figure 3.22: When laser pulses were superimposed on the responses to electric current pulses a reduction in magnitude of action potential was observed. The figures show responses for four different cells, each shown by different color (a) Action potential recorded when cells were stimulated with electric current pulses (180 pA, 300 ms) in a whole-cell current clamp experiment, (b) Action potential recorded when a 120 mW laser pulse was superimposed on the current pulse. The green bar indicates the laser pulse and (c) Action potential recorded after the optical stimulation. Cell action potentials recover back to the original value.
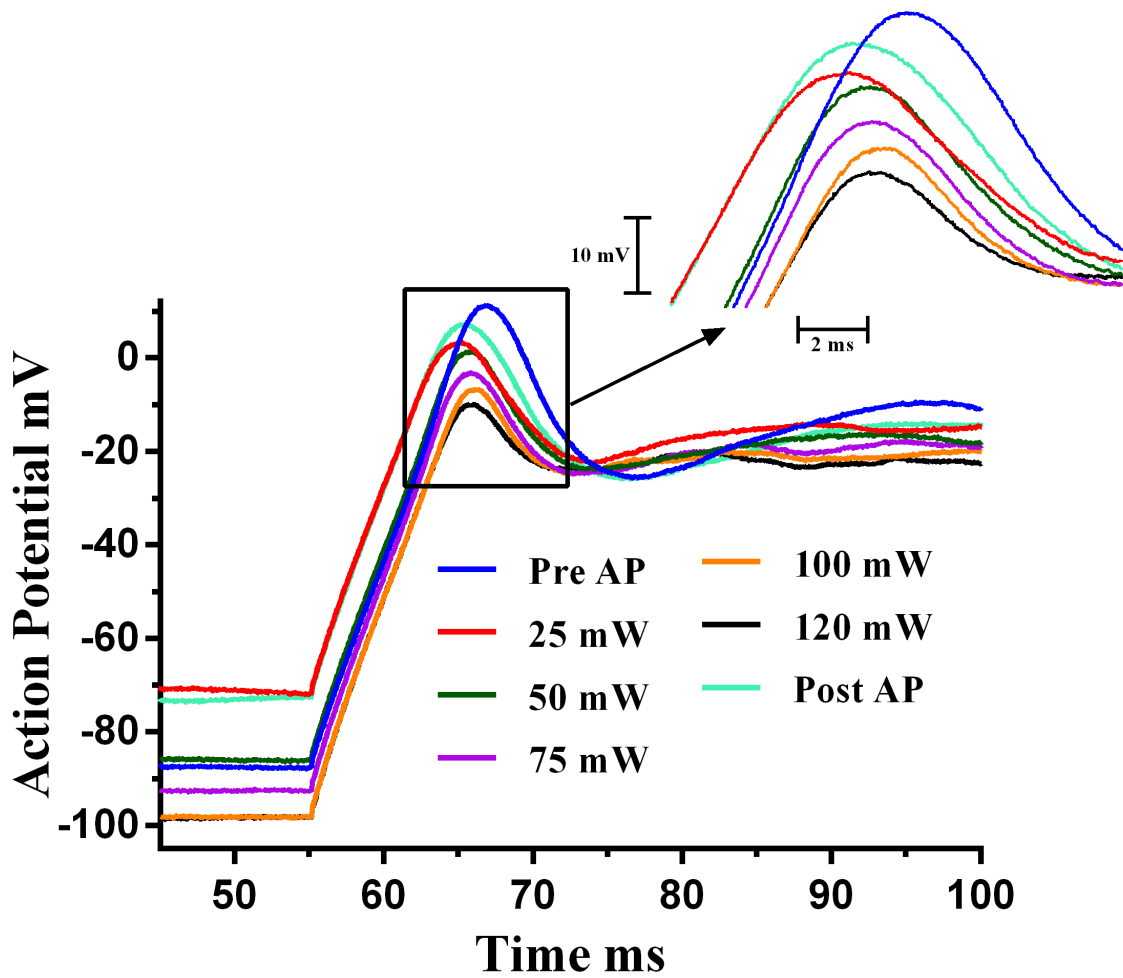
Figure 3.23: The inhibition of action potentials was affected by laser power. As laser power increased, inhibition became more prominent - action potential peak decreased with laser power. The figure shows one such representative SH-SY5Y cell.
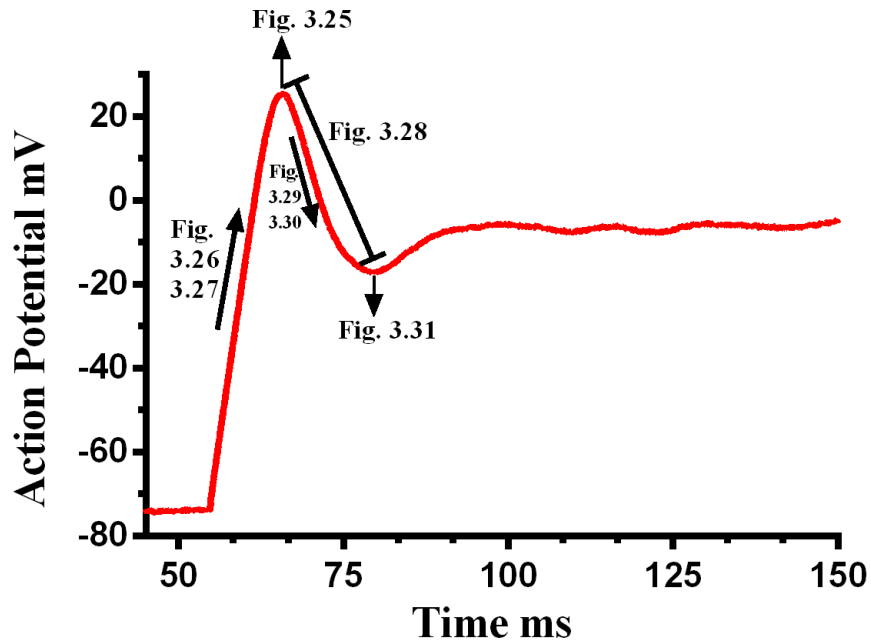
Figure 3.24: A representative figure indicating the various analysis done for inhibition experiments as a function of laser power. These are shown in subsequent figures - Figures 3.25 to 3.31.
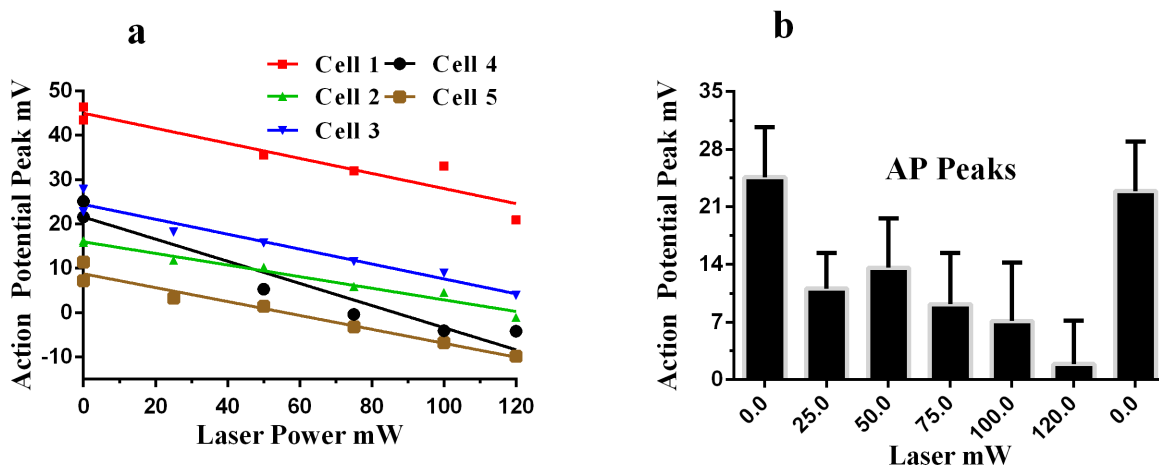
Figure 3.25: Action potential peak decreases as the laser power increased, (a) shown for five different cells and (b), mean values for the same five cells.

43
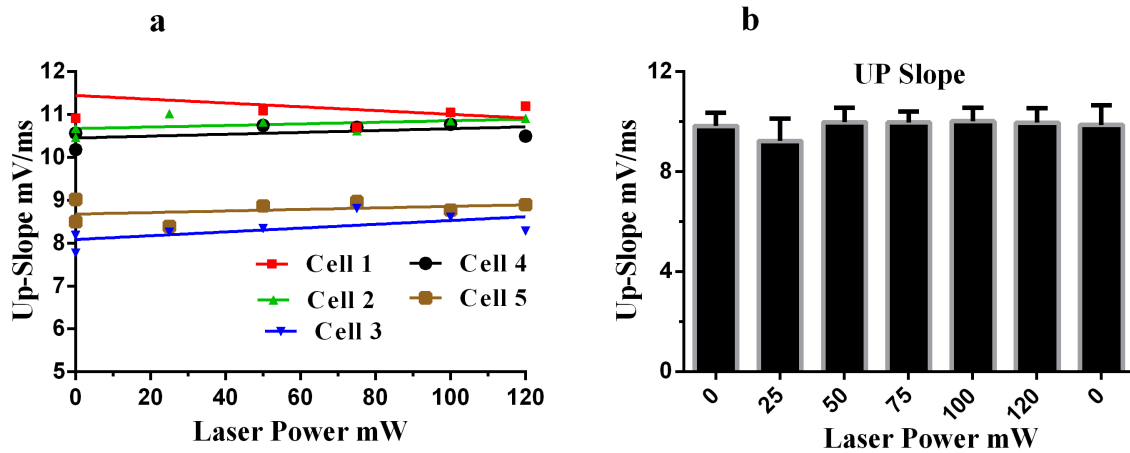
Figure 3.26: The rate of rise of the action potentials (mV/ms) remains unaffected by the laser power. (a) Up-slope vs laser power curves for five different cells. (b) The average values of rate of rise of the action potential versus laser power for five cells.
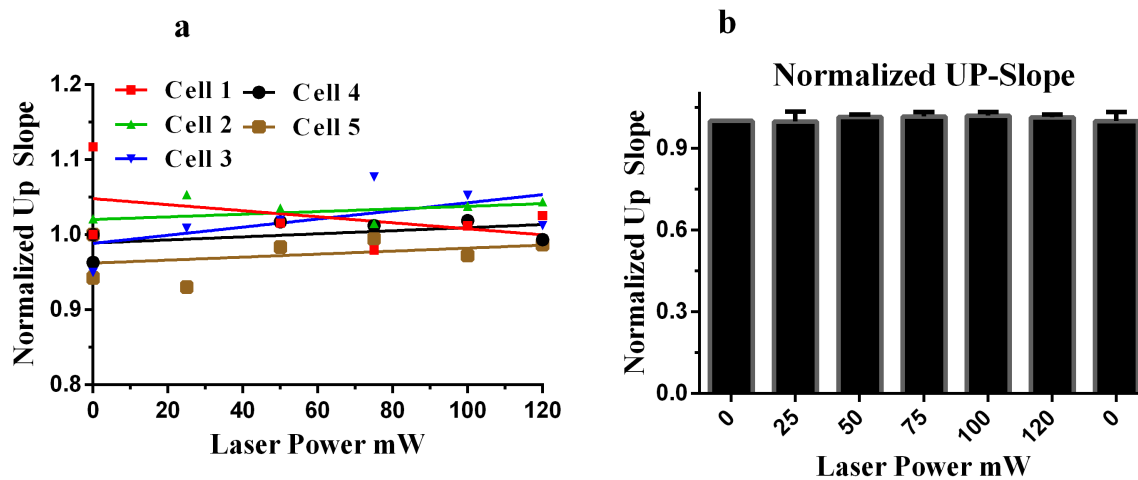
Figure 3.27: Normalized up-slope remains unaffected by laser power. (a) All of the up-slope values were normalized with initial up-slope (Electrical AP up-slope before the laser stimulation experiment) which shows the same trend of having no change with laser power like absolute values. (b) The mean value graph bar confirms the same trend.
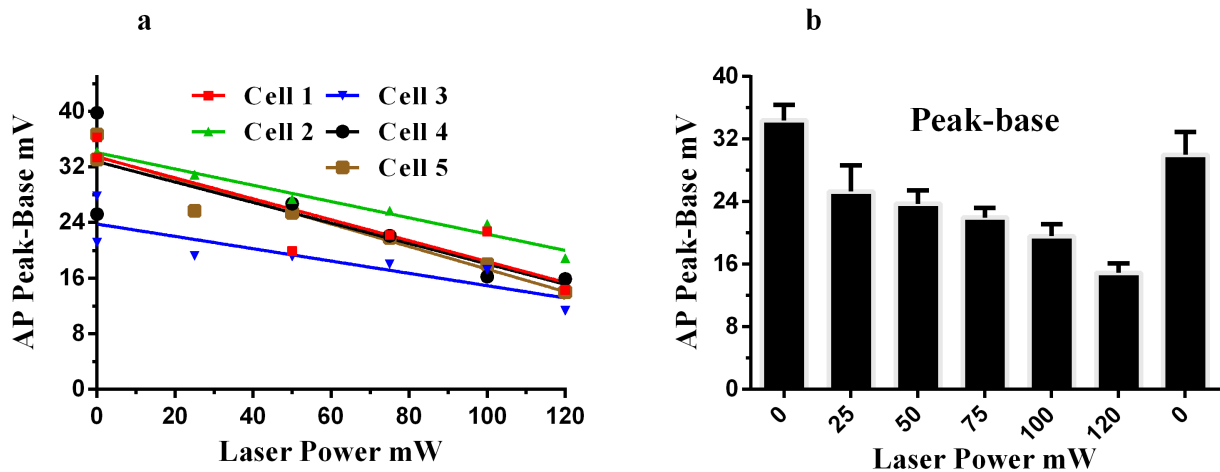
Figure 3.28: The difference between action potential peak and base value (first minima after peak) decreased with laser power. It is due to the decreased in peak values of action potentials being inhibited, as shown by both (a), individual cells and (b), mean values.
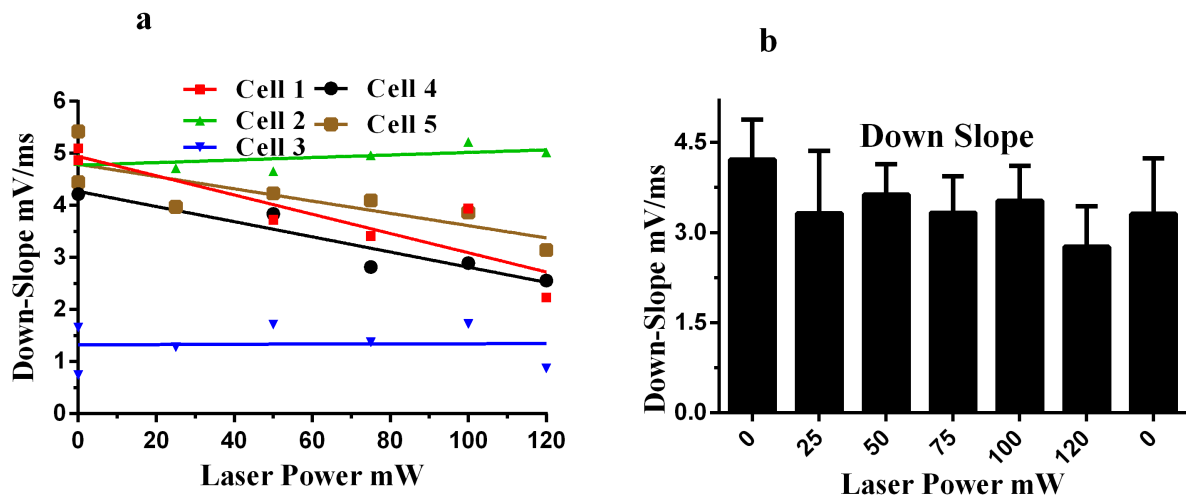
Figure 3.29: The down-slope decreases with laser power as shown in part (a) raw traces for individual five cells and (b) mean values for same five cells.
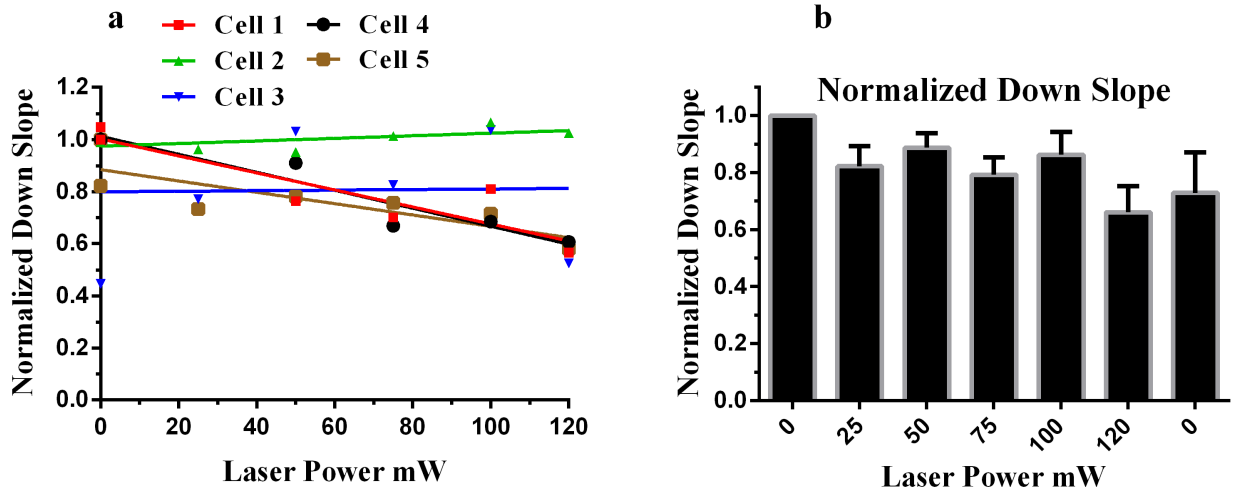
Figure 3.30: Like down-slope, normalized down-slope (down-slopes normalized with downslope of electrical AP down-slope before laser experiment) decreases with laser power. (a) normalized down slope for five cells and (b) mean values [N =5].
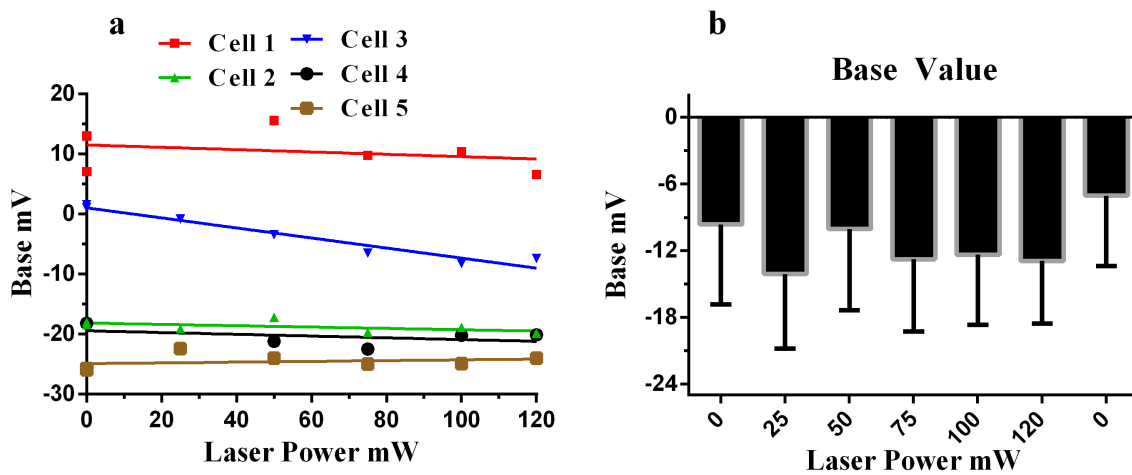
Figure 3.31: The base value (first minima) remains the same, i.e., did not vary with laser power; (a) base values for individual cells and (b) mean data for five cells.

46
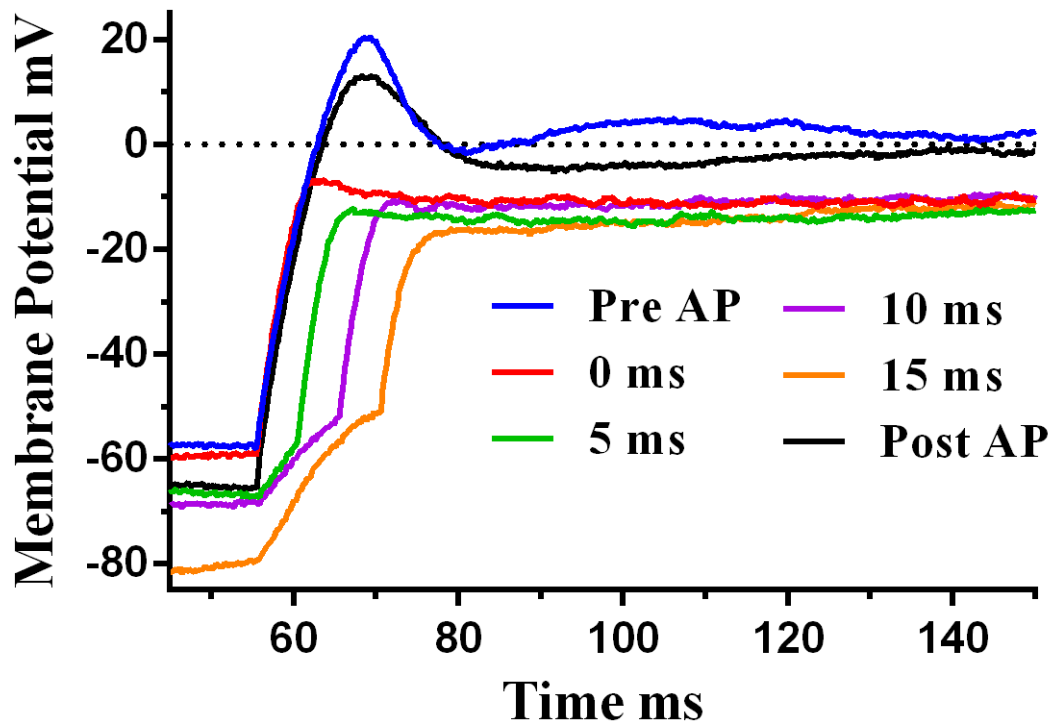
Figure 3.32: The inhibition is more prominent when the laser pulse leads the electrical pulse by a few milliseconds. The figure shows a representative cell where the laser pulse leads the current pulse for three different times: - 5 ms, 10 ms and 15 ms. Action potentials were recorded before (Pre-AP) and after (Post-AP) the optical stimulation experiment.
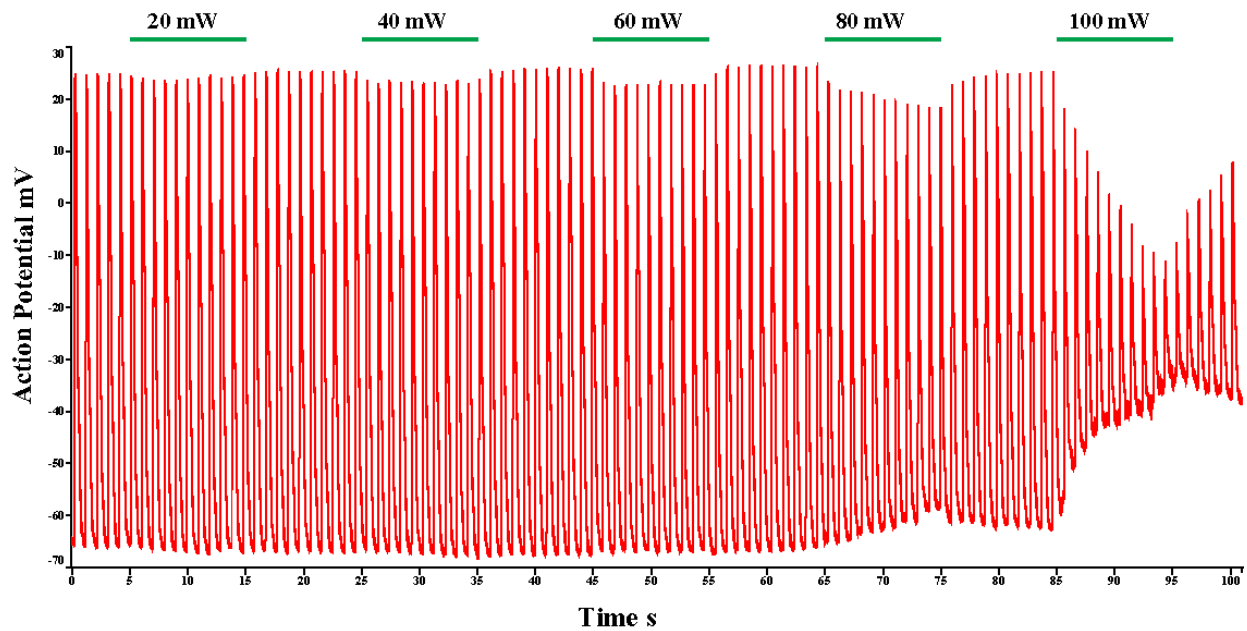
Figure 3.33: Plasmonic stimulation of spontaneous beating cardiomyocytes. Green bars show the laser stimulus pulses. As laser power increases, suppression in magnitude of the action potential becomes more prominent as shown in the figure, with a maximum for the 100 mW laser power.

48
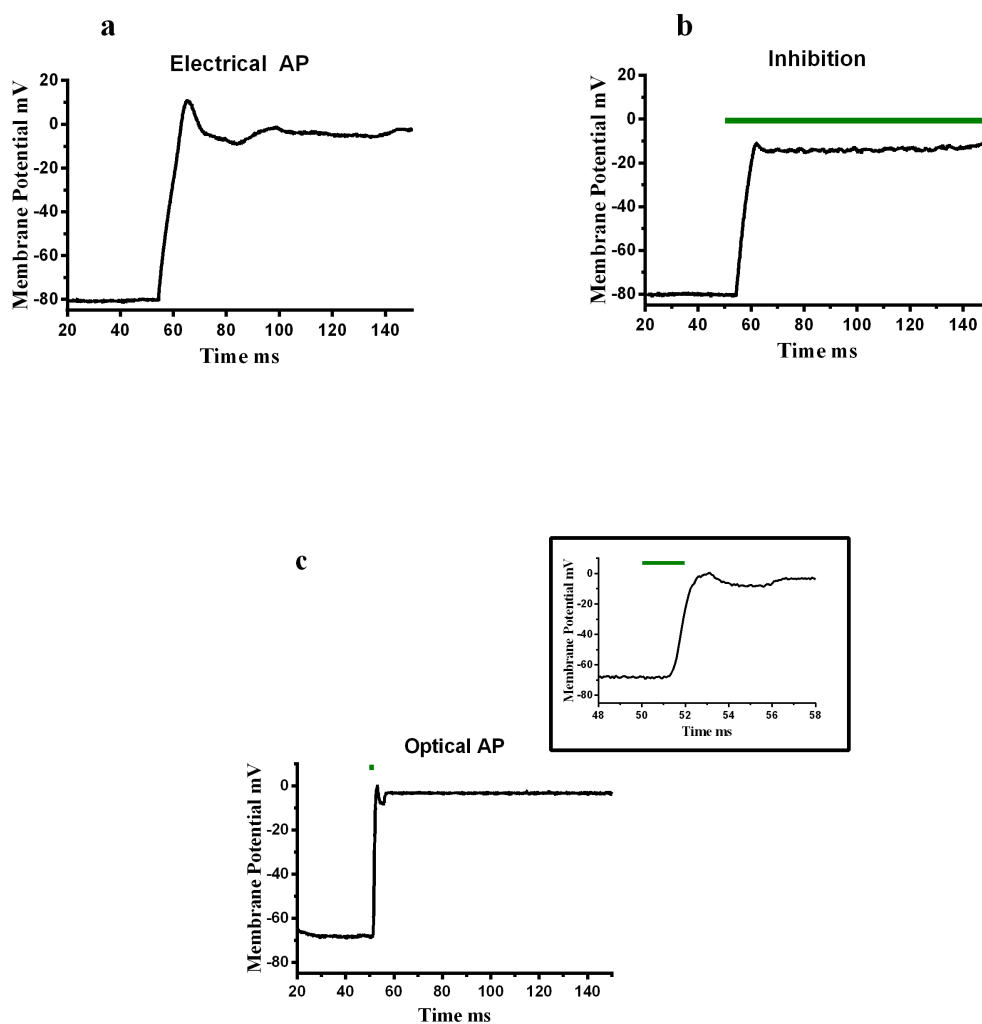
Figure 3.34: Inhibition and activation in response to laser stimulation was recorded from a single cell. (a) Action potential of a representative SH-SY5Y cell in response to 180 pA, 300 ms electrical pulse. Subsequently, inhibition (120 mW, 532 nm green laser pulse was superimposed on the 180 pA electrical pulse) and activation (2 ms, 120 mW laser pulse) in response to laser stimulation were recorded. Part b and c shows the inhibition and activation recordings and inset of part c shows the long time scales of the optical AP.

4 DISCUSSION

To overcome the limitations of clinical electrical stimulation, light stimulation offers exciting opportunities, especially, regarding capabilities of focusing it on small areas at sub-micron levels (Antognazza et al., 2015; Colombo et al., 2016; Shapiro et al., 2012; Wang and Guo, 2016). In the present study, we explored visible light stimulation for cell manipulation using Au nanoparticles. We have developed an Au nanoelectrode and demonstrated that these electrodes in combination with a 532 nm green laser can both stimulate and inhibit neural signals. This the first report showing both inhibition as well as activation of neural response together using Au NPs and green visible light. We were able to record the inhibitory and excitatory responses from the same cell (Figure 3.34). Because of its capabilities to elicit inhibitory and excitatory responses, plasmonic stimulation can be a promising alternative for electrical stimulation paradigms in sensorineural prosthetic and testing devices.

4.1 Neural Activation

When the laser was focused on the nanoelectrode, placed near a patched neuron, a change in cell potential was observed. The laser timing is a critical parameter for eliciting action potentials. The cells fired action potentials for laser pulses of 1-5 ms durations (Figures 3.19, 3.20, 3.21). For larger pulses (time > -10 ms), though there was a shift in cell potential but the response rate was not sufficient to generate action potentials (Figures 3.13, 3.15, 3.16, 3.17). Our findings about pulse duration are consistent with the literature. Eom et al. (2014) showed neural activity enhancement utilizing mid-infrared (980 nm fiber coupled laser) stimulation for rat sciatic nerve when the nerve was stimulated in the presence of gold nanorods, as compared to the control condition (no gold nanorods). 1 μL Au nanorods solution was injected to the sciatic nerve *in-vivo*, subsequently,

50

the close-by area of the excised nerve was illuminated by the laser. There was approximately a six times increase in the magnitude of the compound nerve action potential, with a higher rate of depolarization - 5.7 times higher, when using Au nanorods. The laser pulse durations were a couple of milliseconds (< 3 ms), of the same order in which we observed neural activation (1-5 ms). Similarly, Carvalho-de Souza et al. (2015) reported activation of dorsal ganglion neurons from neonatal rats and acute slices of mouse hippocampus using neurotoxin (TS1) conjugated Au nanoparticles - so, targeting specific ion channels, and a 532 nm green laser. The conjugated nanoparticles showed resistance to the washout. Like Eom et al. (2014) study, laser pulse time was on the order of a millisecond - 1 ms, similar to the range (1-5 ms) for which we recorded action potentials in the current investigation.

4.1.1 Mechanism

Light interaction with gold nanoparticles results in collective oscillations of electrons which have both strong near field and far field affects, specially, for a particular wavelength of light. The near field affects the surroundings of the nanoparticle a distance equal or smaller than the order of the wavelength of the light (Kelly et al., 2003; Lin et al., 2015; Myroshnychenko et al., 2008; Nedyalkov et al., 2007, 2012). Though, the intensity of field is high, it falls off rapidly with distance (Nedyalkov et al., 2012). Since the stimulating nanoelectrode is a few microns (1-3 micron) away from the cells, the electric field is an unlikely contributor for stimulation of the cells. For far fields, Au nanoparticles generate localized thermal fields nearby, especially, for small size particles (< 20 nm) (Coronado et al., 2011; Huang and El-Sayed, 2010). Since we are using particles of approximately 20 nm, it is very likely that localized thermal fields of non-radiative decay (plasmonic heating) play a critical role in the neural stimulation. Localized plasmonic heating could have the similar mechanism as infrared stimulation. It has been demonstrated that pulsed infrared lasers can stimulate various neural cells *in-vivo* and *in-vitro*, e.g., auditory nerve (Izzo et al., 2007b, 2008), peripheral nerve (Wells et al., 2005, 2007a,b), vestibular hair cells (Rajguru et al., 2011),

51

and heart cells (Jenkins et al., 2010). Shapiro et al. (2012) studied the mechanisms of infrared stimulation with Xenopus laevis oocytes, mammalian HEK cells and artificial lipid bilayers, and reported that the absorption of infrared lasers lead to rises in localized temperature which, instead of affecting individual channels, alters the membrane capacitance. The artificial bilayer is considered as a model for cell membrane and capacitance change in response to infrared stimulation. The very likely mechanism is that interactions of visible light with Au NPs results in localized heating around the particles which alters the cell capacitance. Carvalho-de Souza et al. (2015) also attributed the conjugated Au NPs cell activation of dorsal root ganglion neurons to the change in membrane capacitance. Like Shapiro et al. (2012), an artificial lipid bilayer was considered as a representative model of cell membrane capacitance changes. In sum, initial reports suggest that membrane capacitance change is the driving force for action potential generation in response to a thermal pulse. Apart from the transient capacitance change mechanism, there are in-direct indications that heat sensitive channels like TRPV (Caterina et al., 1997; Güler et al., 2002) also plays a role in cell depolarization Richter et al. (2011). Katz et al. (2010) recorded depolarization currents from dorsal root ganglion (DRG) neurons in response an 1889 nm laser. The results were attributed to activation of TRPV1 channels and other channels. It would be worthwhile to further explore the combine effect of heat sensitive channels along with membrane capacitance changes in response to short thermal pulses.

4.2 Neural Inhibition

Along with neural activation, neural inhibition is equally important clinically, and used to inhibit abnormal activities in neurological diseases, e.g., in brain trauma and epilepsy. To test the capability of our nanoelectrode for neural inhibition, laser pulses were superimposed on the electric current pulse and responses were recorded from the SH-SY5Y neurons. A decrease in amplitude of action potentials was observed as compared to control experiments - only current stimulation, no laser stimulation. The pulse duration was 300 ms. Yoo et al. (2014) reported inhibition in neural

activity of Sprague Dawley hippocampal tissue slices when stimulated with gold nanorods and a 785 nm near IR laser. The laser pulse durations were from couple of seconds to a few minutes. In addition, (Yoo et al., 2016) reported an opto-electrical platform made up of a microelectrode array for neural inhibition. The microelectrode arrays were integrated with Au nanorodes and primary hippocampal neurons were cultured on the integrated design. The inhibition was recorded in response to a 785 nm infrared laser having a duration of a few minutes. In present report, we observed a similar inhibition of neural activity in our plasmonic stimulation experiments for 300 ms laser pulses. Similar, inhibition was observed from spontaneously beating neonatal cardiomyocytes when our nanoelectrode was illuminated with 10 s green laser pulses, figure 3.33.

4.2.1 Biological Mechanism

Interestingly, previous reports suggest that inhibition due to thermal pulses is driven by potassium channel currents (Yoo et al., 2014, 2016). Yoo et al. (2014) reported the inhibition of hippocampal neurons in response to illumination of gold nanorods with 785 nm near infrared laser. The inhibition was attributed to the involvement of a thermo-sensitive potassium channel, TREK-1, i.e., photothermal inhibition. When stimulation was carried out with fluoxetine - a TREK-1 blocker, no suppression in neural activity was observed. Rabbitt et al. (2016) demonstrated inhibition in the presence of infrared stimulation with type II vestibular hair cells *ex vivo* from mice, and afferent neurons *in-vivo* from chinchillas. They attributed the excitatory responses to the transient membrane capacitance changes and inhibitory responses were thought to be governed by large conductance Ca^{2+} activated potassium channels, so called BK channels. The application of 100 nM iberiotoxin (IBTX)- a selective blocker of BK channels, eliminated the inhibitory response. This evidence suggests that inhibition could be mediated by heat-sensitive potassium channels like TREK-1 and/or BK. Relevant to the current project, SH-SY5Y cell lines express both TREK-1 (Tong et al., 2013) and BK channels (Curci et al., 2014; Park et al., 2010).

53

One more possible mechanism is the occurrence nanopore formations in the cell membrane, which facilitate the exchange of ions and probably, activates the voltage-gated ion channels as shown by Beier and colleagues (Beier et al., 2014; Olsovsky et al., 2015; Roth et al., 2016; Walsh et al., 2016). Beier et al. (2014) have shown the presence of intracellular responses, such as influx of Ca^{2+} ions due to activation of intracellular pathways, for cells when they were exposed to milliseconds durations of infrared laser pulses. They attributed this influx to nanometer pore formations in the cell membrane. Fluorescent markers were used to study the cell response to IR stimulation. Further studies need to be done to investigate the role of heat-sensitive cell membrane channels in for mechanisms involved in plasmonic neural stimulation.

4.3   Comparison with Other Light Stimulations Methods

Nanomaterial assisted neural stimulation, infrared (Izzo et al., 2006, 2007b; Shapiro et al., 2012; Wells et al., 2005) and optogenetics (Ayling et al., 2009; Boyden et al., 2005; Darrow et al., 2015; Hira et al., 2009; Huff et al., 2013; Shimano et al., 2013), are newer emerging bio-stimulation technologies.

4.3.1   Infrared Stimulation

Infrared stimulation showed potential in stimulation some neural systems both *in vitro* and *in vivo*. For instance, Wells et al. (2005) stimulated rat sciatic nerve *in-vivo* using a tunable laser having wavelength 2 to 10 μm. The compound nerve action potential (CNAP) and compound muscle action potential were recorded. Cayce et al. (2010) demonstrated the feasibility of IR stimulation in central nervous system (CNS) stimulation. Action potentials were recorded form rat thalamocortical brain slices in response to 2.5 μm to 10 μm IR laser. Similarly, Shapiro et al. (2012) stimulated oocytes and HEK cells using IR lasers (1.869 μm for HEK cells and 1.889 μm for oocytes) *in vitro*. The major disadvantage with infrared stimulation is that, along with the neurons,

54

the infrared laser heats up the surrounding tissue as well, which can cause thermal damage and/or unwanted stimulation. As we are using visible light, and due to the localized nature of plasmonic heating in the novel approach of the present investigation, our method would, potentially, overcome these limitations.

4.3.2 Optogenetics

Optogenetics is another light based techniques used to precise control neural excitation and inhibition. For example, Boyden et al. (2005) expressed algae protein Channelrhodopsin-2 (ChR-2) into hippocampal neurons from postnatal day 0 Sprague Dawley rats. When ChR-2 expressed neurons were illuminated with blue light, depolarization currents were observed. ChR2 can genetically target single neurons and this neural activity can be studied. Darrow et al. (2015) used ChR-2 to stimulate the auditory system. ChR-2 channels were expressed in the cochlear nucleus via viral-mediated gene transfer methodologies. The responses recorded from the auditory midbrain - inferior colliculus, when the cochlear nucleus was stimulated with 473 nm pulses (blue laser). The optogenetic technique has the added complexity of requiring genetic manipulation of the target cell population, allowing the cellular machinery to produce light-sensitive ion channels, such as ChR-2. It would be a challenge to achieve clinical transnational prosthetic device stimulation using optogenetics. With our nanoelectrode and visible light, there is no need of genetic modification to achieve neural modulation.

5 FUTURE RECOMMENDATIONS

The developed nanoelectrode, when illuminated with visible light, can stimulate as well inhibit neural signaling. Given these breakthrough results, the future work should focus towards the development of nanomaterials and light-based technologies which could be deployed in various translational modes, such as cochlear implants. One of our proposed designs involves a neural cuff placed around the auditory nerve which will have the nanomaterial coated micro-beads along with the light source Figure 5.1. The substrate or cuff has the potential for carrying several hundred electrodes as compared to a maximum of up to 22 electrodes found in many current cochlear implants (Wilson and Dorman, 2008). The goal would be that the new laser stimulation device would stimulate much more discrete groups of ANFs. More specifically, upcoming work can be divided into two parts - understanding plasmonic stimulation with *in vitro* experiments and *in vivo* applications using animal models with a special focus on cochlear implants.
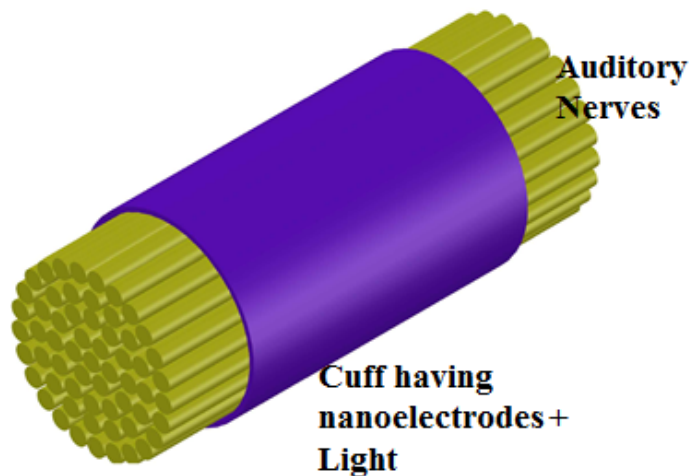
Figure 5.1: Plasmonic based cochlear implant conceptual design, in which nanoelectrodes can be used for stimulation of frequency specific auditory nerve fibers.

5.1 *In-vitro* Experiments

The primary focus of *in vitro* work should be to develop a robust plasmonic stimulation system for electrically excitable biological cells by understanding the biological mechanisms both qualitatively and quantitatively, and establishing nanomaterial/laser parameters for neural stimulation responses. It can be further subdivided into two parts - experiments and mathematical modeling. The different size nanoparticles can be used to develop the nanoelectrodes which stimulate primary neurons, peripheral nerves and cardiomyocytes. This will allow us to optimize the nanoparticle and laser parameters for more controlled and precise plasmonic stimulation. Along with lab experiments, mathematical models can also be used to unravel the physical mechanisms crucial plasmonic neural stimulation. The electrical and thermal fields generated upon visible light interactions with the Au NPs at the nanoelectrode tip upon laser pulsing will be calculated using techniques like finite difference time domain (FDTD) simulations. The obtained results can be adapted for standard Hodgkin-Huxley electrophysiological models to predict the cellular electrical response properties. Along with continuum approach, it will be worthwhile to explore models at molecular levels using techniques like molecular dynamic simulations.

5.2 *In vivo* Applications

Following optimization of NP and laser characteristics, this aim will test the hypothesis that the novel laser/electrode systems can effectively stimulate *in vivo*. To test the initial viability of plasmonic stimulation in vivo, rat sciatic nerve can be stimulated using the optimized NP platform while recording the compound action potential. The sciatic nerve excitation can serve as an initial proof-of-concept for further in vivo studies. Subsequently, plasmonic stimulation could be used to stimulate cochlear neurons in mice while recording responses from the brain; to pave the way for novel sensory implant designs. Plasmonic stimulation experiments with deaf animal models will pave the way for development of plasmonic stimulation-based cochlear implants for deaf people.

6 OUTLOOK

Nanoparticle-assisted neural modulation is still in its early research stages. Most studies are focused on *in vitro* proof-of-concept (Carvalho-de Souza et al., 2015; Eom et al., 2014; Farah et al., 2013; Li et al., 2015; Pappas et al., 2007; Yong et al., 2014; Yoo et al., 2014; Zhao et al., 2009), with very few successful *in vivo* experiments being reported, especially for neural excitation (Chen et al., 2015; Li et al., 2015). Most studies have one common feature in their methodologies, i.e., the modification of nano-neural interfaces to achieve the stimulation. The major drawback with alteration of nano-neural surfaces is that *in vivo* translation raises issues regarding unwanted toxicity, repeatability and bio-compatibility. For example, excessive heating by infrared lasers can damage healthy tissues and produce unwanted excitation or inhibition. Our method of using nanoelectrodes (micro-substrates coated with nanomaterials) which provide a physical buffer between the particles and neural tissue, and optical fibers for delivering visible laser light locally holds much promise for addressing many of these problems. With a nanoelectrode or similar probe, there is no need to attach nanoparticles to the neurons. In addition, as reported here, nanoelectrodes can be easily tested using various methods like light-induced photocurrents (few 100s of nA), fluorescence quenching (emission spectra around 520 nm) and plasmonic temperature jumps (pipette resistance method and infrared thermograms).

Our future studies will be focused on developing more robust plasmonic stimulation systems by better understanding the biological mechanisms involved, and teasing apart the interactions of nanomaterial/laser parameters for controlling neural and cardiac stimulation responses. We will also explore the *in vivo* applications of plasmonic stimulation with an eye towards the development, initially, of plasmonic-based cochlear implants for deaf people. Also, unlike electrical stimulation, plasmonic stimulation does not require any wire connection between nanomaterials and the energy

58

source (light, magnetic fields, and radio waves), so, it embodies a wireless method for neural and cardiac stimulation. Another, more direct method would be adaptation of the currently used electrical stimulation cochlear electrode array with optical fibers replacing the electrical electrodes. In a novel modification of the design, one could structure the electrode to locate polymer-electrode material coated Au NPs very close to the basilar membrane, affording extremely specific stimulation, without thermal damage by the visible light utilized.

6.1 Summary and Conclusions

This project served as initial, *in vitro* proof-of-concept that wireless nanoelectrodes in combination with visible light can be used instead of electrical electrodes or IR lasers, for precise temporal modulation of neural and cardiac cellular responses. Based on these initial breakthrough results, we visualize that future biomedical implants based on SPR phenomena using nanoelectrodes and light will give superior spatial resolution and more clinically useful focal stimulation. Implantable electrodes such as cochlear implant electrode arrays, which use polymeric materials can be designed using the fundamental results demonstrated in the dissertation. Overall, the present report provides fundamental new evidence to support the pursuit of plasmonic stimulation as an alternative approach to conventional electrical neuromodulation, or other emerging modalities, such as IR stimulation in biomedical stimulation devices. Because the novel technology of the current investigation has capabilities to elicit both inhibitory and excitatory responses, utilizing different stimulation parameters, this type of plasmonic stimulation system can be a promising alternative for electrical stimulation paradigms in biological prosthetic implants. As emphasized above, the major disadvantage with IR stimulation is that, along with the target neurons, the IR laser heats up the surrounding tissue as well, which can cause thermal damage and/or unwanted excessive stimulation. By combining visible light, which is minimally absorbed by surrounding tissue and aqueous solutions, with an engineered nanomaterial, we have the potential to achieve a unique, highly localized delivery of energy to the target cells to manipulate their bioelectrical behavior.

59

REFERENCES

Antognazza, M. R., Martino, N., Ghezzi, D., Feyen, P., Colombo, E., Endeman, D., Benfenati, F., and Lanzani, G. (2015). Shedding light on living cells. *Advanced Materials*, 27(46):7662–7669.

Aslan, K., Malyn, S. N., and Geddes, C. D. (2007). Metal-enhanced fluorescence from gold surfaces: Angular dependent emission. *Journal of Fluorescence*, 17(1):7–13.

Aslan, K. and Pérez-Luna, V. H. (2004). Quenched emission of fluorescence by ligand functionalized gold nanoparticles. *Journal of fluorescence*, 14(4):401–405.

Ayling, O. G., Harrison, T. C., Boyd, J. D., Goroshkov, A., and Murphy, T. H. (2009). Automated light-based mapping of motor cortex by photoactivation of channelrhodopsin-2 transgenic mice. *Nature methods*, 6(3):219–224.

Beier, H. T., Tolstykh, G. P., Musick, J. D., Thomas, R. J., and Ibey, B. L. (2014). Plasma membrane nanoporation as a possible mechanism behind infrared excitation of cells. *Journal of neural engineering*, 11(6):066006.

Boyden, E. S., Zhang, F., Bamberg, E., Nagel, G., and Deisseroth, K. (2005). Millisecond-timescale, genetically targeted optical control of neural activity. *Nature neuroscience*, 8(9):1263–1268.

Carvalho-de Souza, J. L., Treger, J. S., Dang, B., Kent, S. B., Pepperberg, D. R., and Bezanilla, F. (2015). Photosensitivity of neurons enabled by cell-targeted gold nanoparticles. *Neuron*, 86(1):207–217.

Caterina, M. J., Schumacher, M. A., Tominaga, M., Rosen, T. A., Levine, J. D., and Julius, D. (1997). The capsaicin receptor: a heat-activated ion channel in the pain pathway. *Nature*, 389(6653):816–824.

Cayce, J. M., Kao, C. C., Malphrus, J. D., Konrad, P. E., Mahadevan-Jansen, A., and Jansen, E. D. (2010). Infrared neural stimulation of thalamocortical brain slices. *IEEE Journal of Selected Topics in Quantum Electronics*, 16(3):565–572.

Chen, R., Romero, G., Christiansen, M. G., Mohr, A., and Anikeeva, P. (2015). Wireless magnetothermal deep brain stimulation. *Science*, 347(6229):1477–1480.

Colombo, E., Feyen, P., Antognazza, M. R., Lanzani, G., and Benfenati, F. (2016). Nanoparticles: a challenging vehicle for neural stimulation. *Frontiers in neuroscience*, 10.

Coronado, E. A., Encina, E. R., and Stefani, F. D. (2011). Optical properties of metallic nanoparticles: manipulating light, heat and forces at the nanoscale. *Nanoscale*, 3:4042–4059.

Crooks, R. M., Zhao, M., Sun, L., Chechik, V., and Yeung, L. K. (2001). Dendrimer-encapsulated metal nanoparticles: synthesis, characterization, and applications to catalysis. *Accounts of Chemical Research*, 34(3):181–190.

Curci, A., Mele, A., Camerino, G. M., Dinardo, M. M., and Tricarico, D. (2014). The large conductance ca2+-activated k+ (bkca) channel regulates cell proliferation in sh-sy5y neuroblastoma cells by activating the staurosporine-sensitive protein kinases. *Frontiers in physiology*, 5.

Daniel, M.-C. and Astruc, D. (2004). Gold nanoparticles: assembly, supramolecular chemistry, quantum-size-related properties, and applications toward biology, catalysis, and nanotechnology. *Chemical reviews*, 104(1):293–346.

Darrow, K., Slama, M., Kozin, E., Owoc, M., Hancock, K., Kempfle, J., Edge, A., Lacour, S., Boyden, E., Polley, D., Brown, M. C., and Lee, D. J. (2015). Optogenetic stimulation of the cochlear nucleus using channelrhodopsin-2 evokes activity in the central auditory pathways. *Brain Research*, 1599:44 – 56.

Deisseroth, K. (2015). Optogenetics: 10 years of microbial opsins in neuroscience. *Nature neuroscience*, 18(9):1213–1225.

61

Dulkeith, E., Morteani, A., Niedereichholz, T., Klar, T., Feldmann, J., Levi, S., Van Veggel, F., Reinhoudt, D., Möller, M., and Gittins, D. (2002). Fluorescence quenching of dye molecules near gold nanoparticles: radiative and nonradiative effects. *Physical review letters*, 89(20):203002.

Dulkeith, E., Ringler, M., Klar, T., Feldmann, J., Munoz Javier, A., and Parak, W. (2005). Gold nanoparticles quench fluorescence by phase induced radiative rate suppression. *Nano Letters*, 5(4):585–589.

Eom, K., Kim, J., Choi, J. M., Kang, T., Chang, J. W., Byun, K. M., Jun, S. B., and Kim, S. J. (2014). Enhanced infrared neural stimulation using localized surface plasmon resonance of gold nanorods. *Small*, 10(19):3853–3857.

Epstein, A. E., DiMarco, J. P., Ellenbogen, K. A., Estes, N. M., Freedman, R. A., Gettes, L. S., Gillinov, A. M., Gregoratos, G., Hammill, S. C., Hayes, D. L., et al. (2008). Acc/aha/hrs 2008 guidelines for device-based therapy of cardiac rhythm abnormalitiesa report of the american college of cardiology/american heart association task force on practice guidelines (writing committee to revise the acc/aha/naspe 2002 guideline update for implantation of cardiac pacemakers and antiarrhythmia devices) developed in collaboration with the american association for thoracic surgery and society of thoracic surgeons. *Journal of the American College of Cardiology*, 51(21):e1–e62.

Farah, N., Zoubi, A., Matar, S., Golan, L., Marom, A., Butson, C. R., Brosh, I., and Shoham, S. (2013). Holographically patterned activation using photo-absorber induced neural? thermal stimulation. *Journal of neural engineering*, 10(5):056004.

Firszt, J. B., Koch, D. B., Downing, M., and Litvak, L. (2007). Current steering creates additional pitch percepts in adult cochlear implant recipients. *Otology & Neurotology*, 28(5):629–636.

Frisina, D. and Frisina, R. D. (1997). Speech recognition in noise and presbycusis: relations to possible neural mechanisms. *Hearing Research*, 106(12):95 – 104.

Güler, A. D., Lee, H., Iida, T., Shimizu, I., Tominaga, M., and Caterina, M. (2002). Heat-evoked activation of the ion channel, trpv4. *Journal of Neuroscience*, 22(15):6408–6414.

Hira, R., Honkura, N., Noguchi, J., Maruyama, Y., Augustine, G., Kasai, H., and Matsuzaki, M. (2009). Transcranial optogenetic stimulation for functional mapping of the motor cortex. *Journal of Neuroscience Methods*, 179(2):258–263. cited By 55.

Hornig, R., Laube, T., Walter, P., Velikay-Parel, M., Bornfeld, N., Feucht, M., Akguel, H., Rssler, G., Alteheld, N., Notarp, D. L., Wyatt, J., and Richard, G. (2005). A method and technical equipment for an acute human trial to evaluate retinal implant technology. *Journal of Neural Engineering*, 2(1):S129.

Huang, H., Delikanli, S., Zeng, H., Ferkey, D. M., and Pralle, A. (2010). Remote control of ion channels and neurons through magnetic-field heating of nanoparticles. *Nature nanotechnology*, 5(8):602–606.

Huang, X. and El-Sayed, M. A. (2010). Gold nanoparticles: optical properties and implementations in cancer diagnosis and photothermal therapy. *Journal of Advanced Research*, 1(1):13–28.

Huff, M., Miller, R., Deisseroth, K., Moorman, D., and LaLumiere, R. (2013). Posttraining optogenetic manipulations of basolateral amygdala activity modulate consolidation of inhibitory avoidance memory in rats. *Proceedings of the National Academy of Sciences of the United States of America*, 110(9):3597–3602. cited By 31.

Izzo, A. D., Richter, C.-P., Jansen, E. D., and Walsh, J. T. (2006). Laser stimulation of the auditory nerve. *Lasers in Surgery and Medicine*, 38(8):745–753.

Izzo, A. D., Suh, E., Walsh, J. T., Whitlon, D. S., Richter, C.-P., and Pathria, J. (2007a). Selectivity of neural stimulation in the auditory system: a comparison of optic and electric stimuli. *Journal of biomedical optics*, 12(2):021008–021008.

Izzo, A. D., Walsh, J. T., Jansen, E. D., Bendett, M., Webb, J., Ralph, H., and Richter, C.-P. (2007b). Optical parameter variability in laser nerve stimulation: a study of pulse duration, repetition rate, and wavelength. *Biomedical Engineering, IEEE Transactions on*, 54(6):1108–1114.

Izzo, A. D., Walsh, J. T., Ralph, H., Webb, J., Bendett, M., Wells, J., and Richter, C.-P. (2008). Laser stimulation of auditory neurons: effect of shorter pulse duration and penetration depth. *Biophysical journal*, 94(8):3159–3166.

Jenkins, M. W., Duke, A. R., Gu, S., Doughman, Y., Chiel, H., Fujioka, H., Watanabe, M., Jansen, E., and Rollins, A. M. (2010). Optical pacing of the embryonic heart. *Nature photonics*, 4(9):623–626.

Johansson, S. (1994). Graded action potentials generated by differentiated human neuroblastoma cells. *Acta Physiologica Scandinavica*, 151(3):331–341.

Kang, J. X., Xiao, Y. F., and Leaf, A. (1995). Free, long-chain, polyunsaturated fatty acids reduce membrane electrical excitability in neonatal rat cardiac myocytes. *Proceedings of the National Academy of Sciences*, 92(9):3997–4001.

Katz, E. J., Ilev, I. K., Krauthamer, V., Weinreich, D., et al. (2010). Excitation of primary afferent neurons by near-infrared light in vitro. *Neuroreport*, 21(9):662–666.

Kelly, K. L., Coronado, E., Zhao, L. L., and Schatz, G. C. (2003). The optical properties of metal nanoparticles: the influence of size, shape, and dielectric environment. *The Journal of Physical Chemistry B*, 107(3):668–677.

Kovalevich, J. and Langford, D. (2013). Considerations for the use of sh-sy5y neuroblastoma cells in neurobiology. In Amini, S. and White, M. K., editors, *Neuronal Cell Culture*, volume 1078 of *Methods in Molecular Biology*, pages 9–21. Humana Press.

Kruis, F. E., Fissan, H., and Peled, A. (1998). Synthesis of nanoparticles in the gas phase for electronic, optical and magnetic applications a review. *Journal of Aerosol Science*, 29(5):511–535.

Lee, S., Cha, E.-J., Park, K., Lee, S.-Y., Hong, J.-K., Sun, I.-C., Kim, S. Y., Choi, K., Kwon, I. C., Kim, K., et al. (2008). A near-infrared-fluorescence-quenched gold-nanoparticle imaging probe for in vivo drug screening and protease activity determination. *Angewandte Chemie*, 120(15):2846–2849.

Li, W., Luo, R., Lin, X., Jadhav, A. D., Zhang, Z., Yan, L., Chan, C.-Y., Chen, X., He, J., Chen, C.-H., et al. (2015). Remote modulation of neural activities via near-infrared triggered release of biomolecules. *Biomaterials*, 65:76–85.

Limb, C. J. and Roy, A. T. (2014). Technological, biological, and acoustical constraints to music perception in cochlear implant users. *Hearing Research*, 308(0):13 – 26. Music: A window into the hearing brain.

Lin, W.-C., Lin, W.-C., Tsai, C.-L., and Lin, K.-P. (2015). Finite-difference time-domain simulation of localized surface plasmon resonance adsorption by gold nanoparticles. In *7th WACBE World Congress on Bioengineering 2015*, pages 138–141. Springer.

Littlefield, P. D., Vujanovic, I., Mundi, J., Matic, A. I., and Richter, C.-P. (2010). Laser stimulation of single auditory nerve fibers. *The Laryngoscope*, 120(10):2071–2082.

Lowe, L. B., Brewer, S. H., Krmer, S., Fuierer, R. R., Qian, G., Agbasi-Porter, C. O., Moses, S., Franzen, S., and Feldheim, D. L. (2003). Laser-induced temperature jump electrochemistry on gold nanoparticle-coated electrodes. *Journal of the American Chemical Society*, 125(47):14258–14259.

Lugo, K., Miao, X., Rieke, F., and Lin, L. Y. (2012). Remote switching of cellular activity and cell signaling using light in conjunction with quantum dots. *Biomedical optics express*, 3(3):447–454.

Marino, A., Arai, S., Hou, Y., Sinibaldi, E., Pellegrino, M., Chang, Y.-T., Mazzolai, B., Mattoli, V., Suzuki, M., and Ciofani, G. (2015). Piezoelectric nanoparticle-assisted wireless neuronal stimulation. *ACS nano*, 9(7):7678–7689.

Myroshnychenko, V., Rodríguez-Fernández, J., Pastoriza-Santos, I., Funston, A. M., Novo, C., Mulvaney, P., Liz-Marzán, L. M., and de Abajo, F. J. G. (2008). Modelling the optical response of gold nanoparticles. *Chemical Society Reviews*, 37(9):1792–1805.

Nath, N. and Chilkoti, A. (2002). A colorimetric gold nanoparticle sensor to interrogate biomolecular interactions in real time on a surface. *Analytical Chemistry*, 74(3):504–509.

Nedyalkov, N. N., Atanasov, P. A., and Obara, M. (2007). Near-field properties of a gold nanoparticle array on different substrates excited by a femtosecond laser. *Nanotechnology*, 18(30):305703.

Nedyalkov, N. N., Dikovska, A. O., Dimitrov, I., Nikov, R., Atanasov, P., Toshkova, R. A., Gardeva, E., Yossifova, L. S., and Alexandrov, M. (2012). Far-and near-field optical properties of gold nanoparticle ensembles reported at the xix international conference on advance laser technologies (alt'11), september 2011, golden sands, bulgaria. *Quantum Electronics*, 42(12):1123.

O'Leary, S. J., Richardson, R. R., and McDermott, H. J. (2009). Principles of design and biological approaches for improving the selectivity of cochlear implant electrodes. *Journal of Neural Engineering*, 6(5):055002.

Olsovsky, C. A., Tolstykh, G. P., Ibey, B. L., and Beier, H. T. (2015). Origins of intracellular calcium mobilization evoked by infrared laser stimulation.

Otsuka, H., Nagasaki, Y., and Kataoka, K. (2003). Pegylated nanoparticles for biological and pharmaceutical applications. *Advanced drug delivery reviews*, 55(3):403–419.

Pappas, T. C., Wickramanyake, W. S., Jan, E., Motamedi, M., Brodwick, M., and Kotov, N. A. (2007). Nanoscale engineering of a cellular interface with semiconductor nanoparticle films for photoelectric stimulation of neurons. *Nano letters*, 7(2):513–519.

Park, J. H., Park, S. J., Chung, M. K., Jung, K. H., Choi, M. R., Kim, Y., Chai, Y. G., Kim, S. J., and Park, K. S. (2010). High expression of large-conductance ca 2+-activated k+ channel in the cd133+ subpopulation of sh-sy5y neuroblastoma cells. *Biochemical and biophysical research communications*, 396(3):637–642.

Phlman, S., Ruusala, A.-I., Abrahamsson, L., Mattsson, M. E., and Esscher, T. (1984). Retinoic acid-induced differentiation of cultured human neuroblastoma cells: a comparison with phorbolester-induced differentiation. *Cell Differentiation*, 14(2):135 – 144.

Rabbitt, R. D., Brichta, A. M., Tabatabaee, H., Boutros, P. J., Ahn, J. H., Della Santina, C. C., Poppi, L., and Lim, R. (2016). Heat pulse excitability of vestibular hair cells and afferent neurons. *Journal of neurophysiology*, pages jn–00110.

Rajguru, S. M., Matic, A. I., Robinson, A. M., Fishman, A. J., Moreno, L. E., Bradley, A., Vujanovic, I., Breen, J., Wells, J. D., Bendett, M., et al. (2010). Optical cochlear implants: evaluation of surgical approach and laser parameters in cats. *Hearing research*, 269(1):102–111.

Rajguru, S. M., Richter, C.-P., Matic, A. I., Holstein, G. R., Highstein, S. M., Dittami, G. M., and Rabbitt, R. D. (2011). Infrared photostimulation of the crista ampullaris. *The Journal of physiology*, 589(6):1283–1294.

Richter, C.-P., Matic, A. I., Wells, J. D., Jansen, E. D., and Walsh, J. T. (2011). Neural stimulation with optical radiation. *Laser & photonics reviews*, 5(1):68–80.

Roth, C. C., Barnes, R. A., Ibey, B. L., Glickman, R. D., and Beier, H. T. (2016). Short infrared (ir) laser pulses can induce nanoporation.

Salameh, A. and Dhein, S. (2005). Culture of neonatal cardiomyocytes. In Dhein, S., Mohr, F., and Delmar, M., editors, *Practical Methods in Cardiovascular Research*, pages 568–576. Springer Berlin Heidelberg.

Salata, O. V. (2004). Applications of nanoparticles in biology and medicine. *Journal of nanobiotechnology*, 2(1):3.

Schneider, G., Decher, G., Nerambourg, N., Praho, R., Werts, M. H., and Blanchard-Desce, M. (2006). Distance-dependent fluorescence quenching on gold nanoparticles ensheathed with layer-by-layer assembled polyelectrolytes. *Nano letters*, 6(3):530–536.

Shapiro, M. G., Homma, K., Villarreal, S., Richter, C.-P., and Bezanilla, F. (2012). Infrared light excites cells by changing their electrical capacitance. *Nature communications*, 3:736.

Shimano, T., Fyk-Kolodziej, B., Mirza, N., Asako, M., Tomoda, K., Bledsoe, S., Pan, Z., Molitor, S., and Holt, A. (2013). Assessment of the aav-mediated expression of channelrhodopsin-2 and halorhodopsin in brainstem neurons mediating auditory signaling. *Brain Research*, 1511:138–152. cited By 13.

Shipway, A. N., Katz, E., and Willner, I. (2000). Nanoparticle arrays on surfaces for electronic, optical, and sensor applications. *ChemPhysChem*, 1(1):18–52.

Tong, L., Cai, M., Huang, Y., Zhang, H., Su, B., Li, Z., and Dong, H. (2013). Activation of k2p channel–trek1 mediates the neuroprotection induced by sevoflurane preconditioning. *British journal of anaesthesia*, page aet338.

Tosetti, P., Taglietti, V., and Toselli, M. (1998). Functional changes in potassium conductances of the human neuroblastoma cell line sh-sy5y during in vitro differentiation. *Journal of Neurophysiology*, 79(2):648–658.

Walsh, A. J., Tolstykh, G. P., Martens, S., Ibey, B. L., and Beier, H. T. (2016). Action potential block in neurons by infrared light. *Neurophotonics*, 3(4):040501.

Wang, Y. and Guo, L. (2016). Nanomaterial-enabled neural stimulation. *Frontiers in Neuroscience*, 10(69).

Wells, J., Kao, C., Jansen, E. D., Konrad, P., and Mahadevan-Jansen, A. (2005). Application of infrared light for in vivo neural stimulation. *Journal of Biomedical Optics*, 10(6):064003–064003–12.

Wells, J., Kao, C., Konrad, P., Milner, T., Kim, J., Mahadevan-Jansen, A., and Jansen, E. D. (2007a). Biophysical mechanisms of transient optical stimulation of peripheral nerve. *Biophysical journal*, 93(7):2567–2580.

Wells, J., Konrad, P., Kao, C., Jansen, E. D., and Mahadevan-Jansen, A. (2007b). Pulsed laser versus electrical energy for peripheral nerve stimulation. *Journal of Neuroscience Methods*, 163(2):326 – 337.

Wilson, B. S. and Dorman, M. F. (2008). Cochlear implants: a remarkable past and a brilliant future. *Hearing research*, 242(1):3–21.

Wilson, B. S., Finley, C. C., Lawson, D. T., Wolford, R. D., Eddington, D. K., and Rabinowitz, W. M. (1991). Better speech recognition with cochlear implants. *Nature*, 352(6332):236–238.

Wood, M. A. and Ellenbogen, K. A. (2002). Cardiac pacemakers from the patients perspective. *Circulation*, 105(18):2136–2138.

Yao, J., Liu, B., and Qin, F. (2009). Rapid temperature jump by infrared diode laser irradiation for patch-clamp studies. *Biophysical journal*, 96(9):3611–3619.

Yong, J., Needham, K., Brown, W. G., Nayagam, B. A., McArthur, S. L., Yu, A., and Stoddart, P. R. (2014). Gold-nanorod-assisted near-infrared stimulation of primary auditory neurons. *Advanced healthcare materials*, 3(11):1862–1868.

Yoo, S., Hong, S., Choi, Y., Park, J.-H., and Nam, Y. (2014). Photothermal inhibition of neural activity with near-infrared-sensitive nanotransducers. *ACS Nano*, 8(8):8040–8049. PMID: 25046316.

Yoo, S., Kim, R., Park, J.-H., and Nam, Y. (2016). Electro-optical neural platform integrated with nanoplasmonic inhibition interface. *ACS nano*, 10(4):4274–4281.

Zhao, Y., Larimer, P., Pressler, R., Strowbridge, B., and Burda, C. (2009). Wireless activation of neurons in brain slices using nanostructured semiconductor photoelectrodes. *Angewandte Chemie International Edition*, 48(13):2407–2410.